Co-regulation of the antagonistic RepoMan:Aurora-B pair in proliferating cells

Maria Giulia Manzione[a], Jan Rombouts[b], Mikhail Steklov[c], Lorenzo Pasquali[d], Anna Sablina[c,e], Lendert Gelens[b,*], Junbin Qian[a,c,f,*], and Mathieu Bollen[a,*]

[a]Laboratory of Biosignaling & Therapeutics, [b]Laboratory of Dynamics in Biological Systems, Department of Cellular and Molecular Medicine, [e]Department of Oncology, and [f]Laboratory for Translational Genetics, Department of Human Genetics, KU Leuven, B-3000 Leuven, Belgium; [c]VIB-KU Leuven Center for Cancer Biology, VIB, 3000 Leuven, Belgium; [d]Dermatology and Venereology Section, Department of Medicine Solna, Karolinska Institutet, SE-17176 Stockholm, Sweden

ABSTRACT **Chromosome segregation during mitosis is antagonistically regulated by the Aurora-B kinase and RepoMan (recruits PP1 onto mitotic chromatin at anaphase)-associated phosphatases PP1/PP2A. Aurora B is overexpressed in many cancers but, surprisingly, this only rarely causes lethal aneuploidy. Here we show that RepoMan abundance is regulated by the same mechanisms that control Aurora B, including FOXM1-regulated expression and proteasomal degradation following ubiquitination by APC/C-CDH1 or SCF^{FBXW7}. The deregulation of these mechanisms can account for the balanced co-overexpression of Aurora B and RepoMan in many cancers, which limits chromosome segregation errors. In addition, Aurora B and RepoMan independently promote cancer cell proliferation by reducing checkpoint-induced cell-cycle arrest during interphase. The co–up-regulation of RepoMan and Aurora B in tumors is inversely correlated with patient survival, underscoring its potential importance for tumor progression. Finally, we demonstrate that high RepoMan levels sensitize cancer cells to Aurora-B inhibitors. Hence, the co–up-regulation of RepoMan and Aurora B is associated with tumor aggressiveness but also exposes a vulnerable target for therapeutic intervention.**

Monitoring Editor
Kerry Bloom
University of North Carolina, Chapel Hill

Received: Dec 13, 2019
Revised: Jan 13, 2020
Accepted: Jan 17, 2020

INTRODUCTION

Aurora B is the catalytic subunit of the Chromosomal Passenger Complex (CPC), a key regulator of chromosome segregation during mitosis (Carmena *et al.*, 2012; Hindriksen *et al.*, 2017). During (pro) metaphase the CPC is enriched at centromeres and destabilizes erroneous interactions between kinetochores (KTs) and spindle microtubules (MTs) through Aurora-B mediated phosphorylation of KT proteins. The resulting unattached KTs initiate spindle assembly checkpoint (SAC) signaling to generate an inhibitor of anaphase. Once sister chromatids are attached to MTs from opposite poles, the bioriented KTs come under tension by the pulling forces exerted by the MTs. This physically separates centromeric Aurora B from its kinetochore substrates, resulting in the stabilization of MT-KT

This article was published online ahead of print in MBoC in Press (http://www.molbiolcell.org/cgi/doi/10.1091/mbc.E19-12-0698) on January 22, 2020.

The authors declare no competing financial interests.

Author contributions: M.G.M. designed and performed all wet-lab experiments and wrote the first version of the manuscript; L.P. performed univariate and multivariate analysis; M.G.M. and M.S. codesigned the in vitro ubiquitination assays; M.S. performed the in vitro ubiquitination experiments; A.S. contributed to Figure 1C and provided reagents for in vitro ubiquitination assays; M.G.M. and J.Q. performed data analysis from the publicly available data sets; J.R. and L.G. designed and analyzed the mathematical model; L.G., J.Q., and M.B. codesigned the experiments and revised the manuscript; M.B. coordinated the team.

*Address correspondence to: Mathieu Bollen (Mathieu.Bollen@kuleuven.be); Lendert Gelens (Lendert.Gelens@kuleuven.be); Junbin Qian (Junbin.Qian@kuleuven.vib.be).

Abbreviations used: ANOVA, analysis of variance; APC/C, anaphase promoting complex/cyclosome; β-gal, β-galactosidase; BSA, bovine serum albumin; CCLE, Cancer Cell Line Encyclopedia; CDK1, cyclin-dependent kinase 1; CIN, chromosomal instability; CPC, chromosomal passenger complex; D, destruction; DIC, differential interference contrast; DN-CUL1, dominant-negative fragment of CULLIN1; Dox, doxycycline; FBS, fetal bovine serum; FCS, fetal calf serum; GDSC, Genomics of Drug Sensitivity in Cancer; GEPIA, Gene Expression Profiling Interactive Analysis; H3T3, H3 at threonine 3; HPA, Human Protein Atlas; KT, kinetochore; MT, microtubule; PBS, phosphate-buffered saline; PFA, paraformaldehyde; PP1, protein phosphatase 1; PP2A, protein phosphatase 2A; RepoMan, recruits PP1 onto mitotic chromatin at anaphase; ROI, region of interest; SAC, spindle assembly checkpoint.

attachments. In addition to its role in chromosome segregation, Aurora B also promotes chromosome condensation and cytokinesis (Carmena *et al.*, 2012), and opposes cell-cycle arrest and apoptosis in interphase through phosphorylation-dependent degradation of the tumor suppressor p53 (Wu *et al.*, 2011; Gully *et al.*, 2012; González-Loyola *et al.*, 2015). Owing to its pleiotropic function, Aurora B inhibition causes aneuploidy, polyploidy, and subsequent cell death, providing a rationale for clinical trials of small-molecule inhibitors as target therapy (Löwenberg *et al.*, 2011; Schwartz *et al.*, 2013; Mross *et al.*, 2016; Borisa and Bhatt, 2017; Tang *et al.*, 2017).

Aurora B is regulated at different levels. The expression of the Aurora-B gene (*AURKB*) during S-phase is kept low because of degradation of *AURKB* transcripts via the CCR4-NOT deadenylation complex (Rambout *et al.*, 2016). Aurora-B levels maximally increase during G2/M phase when FOXM1 binds to the promoter region of *AURKB* (Wang *et al.*, 2005; Bonet *et al.*, 2012; Fischer *et al.*, 2016a). The Aurora-B protein is targeted for proteasomal degradation following its ubiquitination by anaphase promoting complex/cyclosome (APC/C)-CDH1 at the mitotic exit (Stewart and Fang, 2005) and by SCF^{FBXW7} in interphase (Teng *et al.*, 2012). The activity of Aurora B is also acutely regulated (Carmena *et al.*, 2012; Hindriksen *et al.*, 2017). It is activated by association with CPC components as well as by autophosphorylation in *trans*, which is triggered by its enrichment at centromeres (Sessa *et al.*, 2005; Kelly *et al.*, 2007). In addition, Aurora B is activated by other kinases. Cyclin-dependent kinase 1 (CDK1), the master regulator of mitosis, promotes the centromeric targeting of the CPC through phosphorylation of the regulatory subunit Borealin, which mediates binding to the centromeric protein Shugoshin (Tsukahara *et al.*, 2010). CDK1 also activates Haspin (Zhou *et al.*, 2014), which phosphorylates histone H3 at threonine 3 (H3T3) to create a docking site for the CPC component Survivin (Kelly *et al.*, 2010). In addition, Aurora B and Haspin activate each other, thus generating a positive feedback loop (Wang *et al.*, 2011). Aurora-B signaling is opposed by pools of protein phosphatase 1 (PP1) and protein phosphatase 2A (PP2A)-B56 that are recruited by proteins at the KTs (such as KNL1 for PP1; BUBR1 for PP2A-B56) (Nijenhuis *et al.*, 2014) or chromosome arms (for example, RepoMan [recruits PP1 onto mitotic chromatin at anaphase]) (Trinkle-Mulcahy *et al.*, 2006; Qian *et al.*, 2013).

RepoMan, encoded by *CDCA2*, is a scaffold for protein phosphatases PP1 and PP2A-B56 (Prévost *et al.*, 2013; Qian *et al.*, 2013). RepoMan-associated PP1 dephosphorylates H3T3 during (pro)metaphase to oppose the recruitment of the CPC to the chromosome arms (Qian *et al.*, 2011, 2013). However, centromeric H3T3 is protected from dephosphorylation by PP1-RepoMan because Aurora B locally phosphorylates RepoMan at serine 893 (S893) and threonine 394 (T394), thereby opposing histone and PP1 binding, respectively (Qian *et al.*, 2013; Kumar *et al.*, 2016). This reciprocal regulation, where Aurora B activates the kinase Haspin and inhibits its counteracting phosphatase PP1-RepoMan, contributes to the centromeric enrichment of the CPC in (pro)metaphase. Like Aurora B, RepoMan is also regulated by CDK1 (Qian *et al.*, 2015). Phosphorylation of RepoMan at several sites by CDK1 reduces the binding of PP1 to levels that are still sufficient to keep H3T3 dephosphorylated at the chromosome arms but inadequate to dephosphorylate mitotic exit and interphase substrates. In addition, CDK1 phosphorylates RepoMan at serine 591 (S591) to promote the recruitment of PP2A-B56, which then reverses phosphorylation of S893 by Aurora B to set the level of association of RepoMan with the chromosome arms. After inactivation of CDK1 in early anaphase RepoMan is dephosphorylated, resulting in the loss of PP2A-B56, the massive recruitment of PP1 and the bulk targeting of PP1-RepoMan to the chromosomes. PP1-RepoMan then dephosphorylates a host of other proteins needed for anaphase progression (Wurzenberger *et al.*, 2012), nuclear envelope reassembly (Vagnarelli *et al.*, 2011), and heterochromatin organization (De Castro *et al.*, 2017). In addition, PP1-RepoMan inactivates the DNA-damage checkpoint kinase ATM during interphase and in this way increases the threshold for ATM signaling (Peng *et al.*, 2010; Uchida *et al.*, 2013).

Aurora B is up-regulated in various cancers due to increased FOXM1-mediated transcription of *AURKB* and stabilization of Aurora-B protein through reduced ubiquitination-mediated proteasomal degradation (Nguyen *et al.*, 2005; Stewart and Fang, 2005; Bonet *et al.*, 2012; Teng *et al.*, 2012). Intriguingly, the level of the counteracting RepoMan is also up-regulated in tumors (Krasnoselsky *et al.*, 2005; Ryu *et al.*, 2007; Zhou *et al.*, 2010; Lagarde *et al.*, 2013; Uchida *et al.*, 2013; Lv *et al.*, 2017; Shi *et al.*, 2017; Phan *et al.*, 2018), but it is unclear to which extent Aurora B and RepoMan are co-overexpressed. By comparing the determinants of RepoMan and Aurora-B abundance, we found that they co-oscillate during the cell cycle and are co–up-regulated in many tumors, essentially because they are regulated by the same (post)transcriptional control mechanisms. We also found that the co–up-regulation of RepoMan and Aurora B correlates with tumor progression. Finally, our studies revealed that tumor cells are more sensitive to Aurora-B inhibitors when RepoMan is overexpressed and even more when both Aurora B and RepoMan are co–up-regulated, which can possibly be exploited to stratify patients for Aurora–B-directed cancer therapies.

RESULTS

RepoMan and Aurora B are co-overexpressed in various cancers

To examine the extent to which *AURKB* and *CDCA2* are co-overexpressed in tumors, we first made use of publicly available cancer data sets. The *CDCA2* and *AURKB* transcript levels were increased in all four tumor sets for which sufficient data with matched normal tissues ($n \geq 50$) were available in the Gene Expression Profiling Interactive Analysis (GEPIA) database (Figure 1A). Also, the *CDCA2* and *AURKB* transcript levels were positively correlated in various tumor types, including breast invasive carcinoma (Figure 1B and Supplemental Figure S1A), and more than 1100 cancer cell lines from the Cancer Cell Line Encyclopedia (CCLE) (Supplemental Figure S1A), indicating that co–up-regulation of *CDCA2* and *AURKB* is a common feature of cancer cells. Proteomic analyses of TCGA breast cancer samples also disclosed a strong positive correlation between RepoMan and Aurora-B protein levels (Figure 1C) and immunohistochemical data from the Human Protein Atlas (HPA) database showed a co–up-regulation of RepoMan and Aurora B in choloangiocarcinoma tissue sections (Figure 1, D and E). Finally, an Oncoprint analysis (cBioPortal) revealed that the co-overexpression of *CDCA2* and *AURKB* was not due to an increased gene copy number, which indeed rarely co-occurred in the examined tumors (Figure 1F).

To explore the possible impact of co-overexpression of *CDCA2* and *AURKB* on cancer progression, we examined the relationship between their expression and patient survival in the four cancer types shown in Figure 1A. Kaplan–Meier survival curves showed the shortest survival for patients where both genes were overexpressed (Figure 1G; Supplemental Figure S1, B–D). For the latter patients, the median survival was indeed considerably shorter than that of patients where neither *CDCA2* nor *AURKB* were up-regulated (Supplemental Figure S1, B–D). In lung adenocarcinoma and liver hepatocellular carcinoma, survival of patients with up-regulation of both

CDCA2 and *AURKB* was also significantly shorter than that of patients in which both genes were down-regulated. (Figure 1G and Supplemental Figure S1, C and D). These data indicate that the co–up-regulation of *CDCA2* and *AURKB* in liver and lung cancer is associated with a more aggressive tumor phenotype.

The expression of RepoMan is cell-cycle regulated

To explore the molecular basis of the co–up-regulation of RepoMan and Aurora B in cancer cells, we first compared their expression in normal lung fibroblasts (WI-38) and lung cancer cells (A549). In accordance with the data from tumor samples (Figure 1 and Supplemental Figure S1), RepoMan and Aurora-B protein levels were higher in cancer cells than in nontransformed cells (Figure 2A). Moreover, in both cell lines RepoMan and Aurora-B levels were much higher in prometaphase-arrested cells than in nonsynchronized cells, hinting at a cell cycle-dependent regulation. A similar cell cycle- and tumor cell-dependent RepoMan:Aurora-B co-regulation was also noted for other (non)cancer cells, that is, RPE1, HeLa, and U2OS cells (Supplemental Figure S2A). Importantly, immunostainings disclosed a significant positive correlation between RepoMan and Aurora-B levels in individual A549 cells in prophase (Figure 2, B and C), showing that their co–up-regulation is not explained by overexpression of either Aurora B or RepoMan in distinct subpopulations of cells. Using publicly available data sets (Jerby-Arnon *et al.*, 2018; Zheng *et al.*, 2018), such a correlation was also observed in human hepatocellular carcinoma and melanoma at the single-cell transcriptomic level (Supplemental Figure S2B).

By analyzing the CycleBase data set (Whitfield *et al.*, 2002; Santos *et al.*, 2015), we confirmed that the *CDCA2* and *AURKB* transcript levels co-oscillate in HeLa cells and are low in G1, increased in S phase, and maximal in G2/M (Figure 2D). We also examined the cell cycle-dependent oscillation of RepoMan and Aurora-B proteins following the release of U2OS cells from a double–thymidine-induced G1/S arrest (Figure 2, E and F). After this release, the levels of RepoMan and Aurora B gradually increased until 12–14 h when the cells had accumulated in G2/M, as indicated by the hyperphosphorylation of histone H3 at serine 10 (H3S10ph).

The molecular mechanisms underlying the cell cycle-dependent regulation of the Aurora-B transcript and protein levels are well understood (see the *Introduction*). We sought to obtain similar insights for RepoMan using U2OS cells, which are commonly used to explore cell-cycle regulation (Whitfield *et al.*, 2002). To study the fate of RepoMan after mitosis, prometaphase-arrested U2OS cells were released into fresh medium without nocodazole (Supplemental Figure S2C). RepoMan protein was largely lost within 5 h after the release. Many proteins that accumulate during M-phase, including Aurora B, are targeted for proteasomal degradation at the mitotic exit and/or subsequent G1. We found that the addition of the proteasome inhibitor MG132 resulted in the stabilization of RepoMan and Aurora B in nonsynchronized cells (Figure 2, G and H), suggesting that they are degraded by the proteasomal pathway. The concentration of RepoMan increased up to threefold after the addition of MG132, hinting at a rapid turnover of RepoMan. The half-life of RepoMan was approximately 4–6 h, as derived from its partial disappearance in the presence of the translation inhibitor cycloheximide. Collectively, our data indicated that a dynamic, cell cycle-regulated balance of transcript accumulation and protein degradation determines the abundance of RepoMan protein, similar to what has been reported for Aurora B (Kimura *et al.*, 2004; Stewart and Fang, 2005). These findings prompted us to further explore the mechanisms underlying the expression and destabilization of RepoMan.

FOXM1 regulates *CDCA2* expression

CDCA2 and *AURKB* are both late cell-cycle genes (Kimura *et al.*, 2004; Davis *et al.*, 2010; Müller *et al.*, 2014; Santos *et al.*, 2015; Figure 2, D–F). Such genes are maximally expressed in G2/M and their expression is often stimulated by the transcription factor FOXM1 (Müller *et al.*, 2014; Fischer *et al.*, 2016b). *AURKB* is a well-established target of FOXM1 (Wang *et al.*, 2005; Bonet *et al.*, 2012; Fischer *et al.*, 2016a). We noted that the promoter region of *CDCA2* in mammals also harbors a conserved FOXM1 consensus binding site, known as "cell cycle genes homology region" (Supplemental Figure S3A). Accordingly, *CDCA2* was recently identified as a target of FOXM1 by analyzing 23 ChIP-seq experiments from eight human cancer cell lines (Wang *et al.*, 2017). Also, the level of *FOXM1* and *CDCA2* or *AURKB* transcripts was positively correlated in eight cancer types (Figure 3A) and a collection of more than 1100 human cancer cell lines from CCLE (Supplemental Figure S3B) (Barretina *et al.*, 2012). Consistent with *CDCA2* and *AURKB* being FOXM1-target genes, the small interfering RNA (siRNA)-mediated knockdown of FOXM1 significantly reduced the levels of both RepoMan and Aurora-B protein in cells arrested in mitosis (Figure 3, B and C). However, the latter finding does not rule out the possibility that the loss of RepoMan and Aurora B was (partially) caused by cell-cycle defects associated with the depletion of FOXM1. To examine more directly whether FOXM1 was bound to the promoter region of *CDCA2* and *AURKB*, we performed ChIP-quantitative PCR (qPCR) assays, which confirmed that FOXM1 was associated with the promoter of both *CDCA2* and *AURKB* (Figure 3D). While these data indicate that FOXM1 promotes the expression of *CDCA2* during G2/M, they do not rule out a contribution of additional transcription factors or transcript decay factors to the cell cycle-dependent oscillation of RepoMan transcript (Figure 2D).

Since *CDCA2* and *AURKB* are FOXM1 target genes it could be argued that the effect of their co–up-regulation on patient survival (Figure 1G and Supplemental Figure S1, B–D) was an indirect effect of *FOXM1* up-regulation. Univariate and multivariate analysis confirmed a reduced overall survival probability for liver and lung cancer patients with high *CDCA2* + *AURKB* expression, as compared with patients with low expression of both genes (95% confidence interval [CI], 0.11–1.3; 95% CI, 0.21–1.6) (Figure 3E and Supplemental Figure S3C). However, the co-overexpression of *CDCA2* + *AURKB* + *FOXM1* did not further increase the hazard risk (Figure 3E), suggesting that *CDCA2* + *AURKB* up-regulation, in liver and lung cancer, possibly contributes to poor prognosis, independent of *FOXM1* overexpression.

APC/C-CDH1 targets RepoMan for proteasomal degradation at the mitotic exit

The APC/C is an E3-type ubiquitin ligase that controls the specific and ordered degradation of many mitotic regulators, including Aurora B (Stewart and Fang, 2005; Thornton and Toczyski, 2006; Pines, 2011). It forms distinct functional complexes with the substrate adaptors CDC20 and CDC20 homologue 1 (CDH1) during early/mid-mitosis and late mitosis/early G1, respectively (Peters, 2006). To examine whether the APC/C contributes to the rapid degradation of RepoMan, we first asked whether RepoMan associates with CDC20 and/or CDH1. For this purpose, HEK293T cells were transfected with expression vectors for EGFP-RepoMan with a mutated histone binding site (S893D) or EGFP-β-galactosidase (β-gal; negative control) and either HA-tagged CDC20 or HA-tagged CDH1. Immunoblot analysis of the EGFP traps revealed RepoMan binding to HA-CDH1, but barely so to HA-CDC20 (Figure 4A). This prompted us to examine whether RepoMan is a substrate for ubiquitination by APC/C-CDH1. Purified recombinant His-tagged RepoMan was indeed ubiquitinated by purified APC/C in the presence of CDH1,

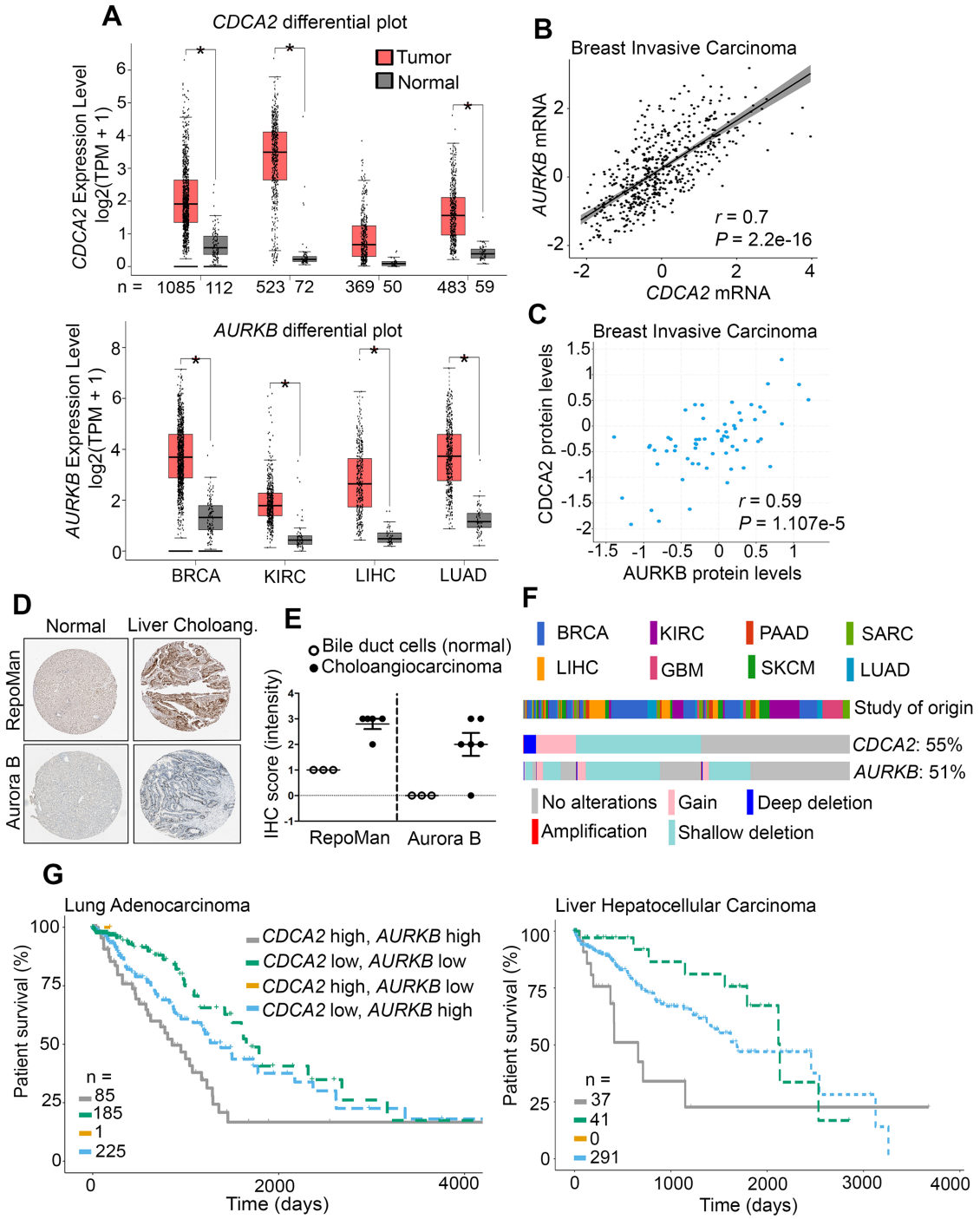

FIGURE 1: High levels of RepoMan and Aurora B predict poor outcome in cancer patients. (A) *CDCA2* and *AURKB* expression in different cancer types and adjacent normal tissues. The box plot is based on data from TCGA and is generated using the GEPIA database. Data are presented as log2 (TPM, transcripts per million +1; $^*P < 0.01$ using the one-way ANOVA test). BRCA, breast invasive carcinoma; KIRC, kidney renal clear cell carcinoma; LIHC, liver hepatocellular carcinoma; LUAD, lung adenocarcinoma. (B) Scatter plot showing the Pearson correlation analysis between *CDCA2* and *AURKB* expression in breast invasive carcinoma (TCGA, provisional). mRNA expression data (array z-score) of *CDCA2* and *AURKB* were obtained from human cancer data sets in the cBioPortal database. *r*, Pearson's correlation coefficient; *P* values for paired *t* test. (C) Correlation between CDCA2 and AURKB protein expression levels in the BRCA TCGA tumors. Protein abundances were determined by mass spectrometry (the National Cancer Institute Clinical Proteomic Tumor Analysis Consortium). *r*, Pearson's correlation coefficient; *P* values for paired *t* test. (D) Representative immunostained tissue sections from normal liver tissue (RepoMan, Patient ID: 3402; Aurora B, Patient ID: 1720) and liver cholangiocarcinoma (Patient ID: 2279) in the HPA. IHC staining were performed with the antibodies HPA030049 (RepoMan) and CAB005862 (Aurora B). (E) The dot plot shows a semi-quantitative analysis of RepoMan and Aurora-B staining intensity (the values strong, moderate, weak, and negative that are used to describe intensity were transformed into 3, 2, 1, and 0, respectively) among three normal cases and ≥5 samples of liver choloangiocarcinoma

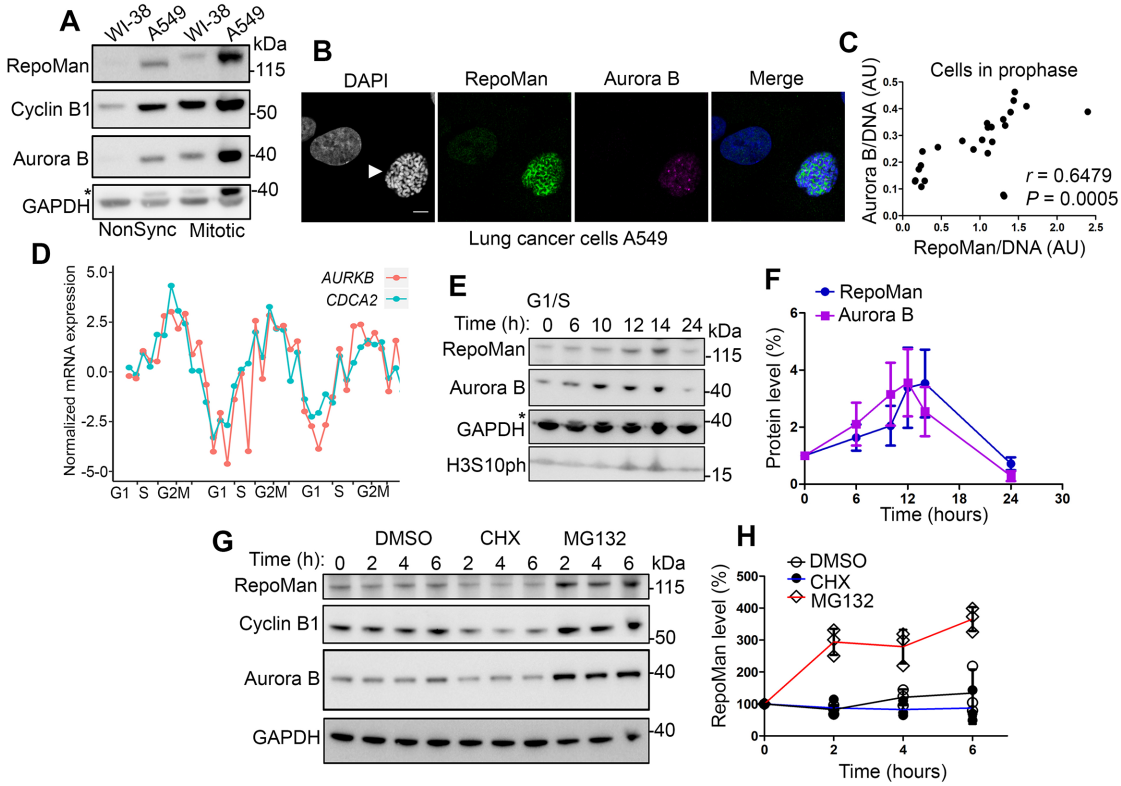

FIGURE 2: The expression of RepoMan is cell-cycle regulated. (A) WI-38 and A549 cells were either nonsynchronized (NonSync) or arrested in prometaphase (Mitotic) by nocodazole arrest. Cell lysates were used for immunoblotting. GAPDH served as loading control (*the residual band is Aurora B after reprobe of the blot for GAPDH). (B) Representative immunofluorescence images of nonsynchronized A549 cells. The white arrow indicates an example of early prophase cell (identified by chromosome condensation within an intact nuclear envelope; Kireeva *et al.*, 2004). Scale bar, 5 μM. (C) Pearson correlation analysis of Aurora-B and RepoMan levels quantified by immunostaining in single prophase A549 cells. *r*, Pearson's correlation coefficient; *P* values for paired *t* test. Each individual dot represents the signal of the mean pixel intensities of RepoMan or Aurora B normalized to DAPI (DNA). The scatter plot shows values obtained from 7–10 prophase cells from each of three independent experiments. (D) Line plot of normalized mRNA expression profiles of *CDCA2* and *AURKB* in HeLa cells at different cell-cycle phases, as obtained from the CycleBase data set. The *y*-axis indicates normalized mRNA expression data plotted on time scale. The *x*-axis indicates different phases of the cell cycle. (E) U2OS cells were arrested at the G1/S boundary with a double-thymidine block, released into fresh medium and harvested at the indicated times. Cell lysates were analyzed by immunoblotting (*the residual band is Aurora B after reprobe of the blot for GAPDH). (F) Quantification of RepoMan and Aurora B protein abundance from four technical replicates performed as in E. RepoMan and Aurora-B band intensities were quantified and normalized to GAPDH and to 0 h. Curves indicate mean percentages ± SD. (G) Nonsynchronized U2OS cells were treated with DMSO (vehicle), cycloheximide (CHX), or MG123 and harvested at the indicated times for immunoblotting. (H) Quantification of RepoMan protein abundance from three experiments performed as in G. RepoMan band intensities were quantified and normalized to GAPDH and to the control (DMSO at 0 h) for three replicates. Curves indicate mean percentages ± SD.

as shown by both RepoMan and ubiquitin blots (Figure 4B). To delineate the biological consequence of the APC/C-CDH1-mediated ubiquitination of RepoMan, we subsequently examined how the RepoMan level is affected by changing the cellular concentration of CDH1. The overexpression of HA-CDH1 resulted in a reduced (61 ± 13% of control; $n = 3$) level of RepoMan (Figure 4C), while the knockdown of endogenous CDH1 caused its stabilization in both nonsynchronized cells (Figure 4D) and following the release from a nocodazole arrest (Supplemental Figure S4, A and B). However, CDH1 overexpression or depletion did not affect the RepoMan transcript level (Supplemental Figure S4, C and D). To explore whether the increase in RepoMan level upon depletion of CDH1 is an indirect effect of a cell-cycle arrest, we performed live imaging of HeLa cells that inducibly express mClover-tagged RepoMan before and after

from the HPA. (F) The OncoPrint from cBioPortal shows genetic alterations in *CDCA2* and *AURKB* in 1960 (70%) out of 2815 patients with the indicated cancers. GBM, glioblastoma multiforme; PAAD, pancreatic adenocarcinoma; SKCM, skin cutaneous melanoma; SARC, sarcoma. Percentages on the right refer to genetic alterations in *CDCA2* (55%) and *AURKB* (51%). Gain: low-level gene amplification event; amplification: high-level gene amplification event; deep deletion: homozygous (total) loss; shallow deletion: heterozygous deletion. (G) Kaplan–Meier plots comparing survival of patients with combined high and/or low expression of *CDCA2* and *AURKB*, based on TCGA data for the indicated cancers. Survival analysis showing the effects of *CDCA2* or *AURKB* alone for liver and lung cancer patients are shown in Supplemental Figure S3C.

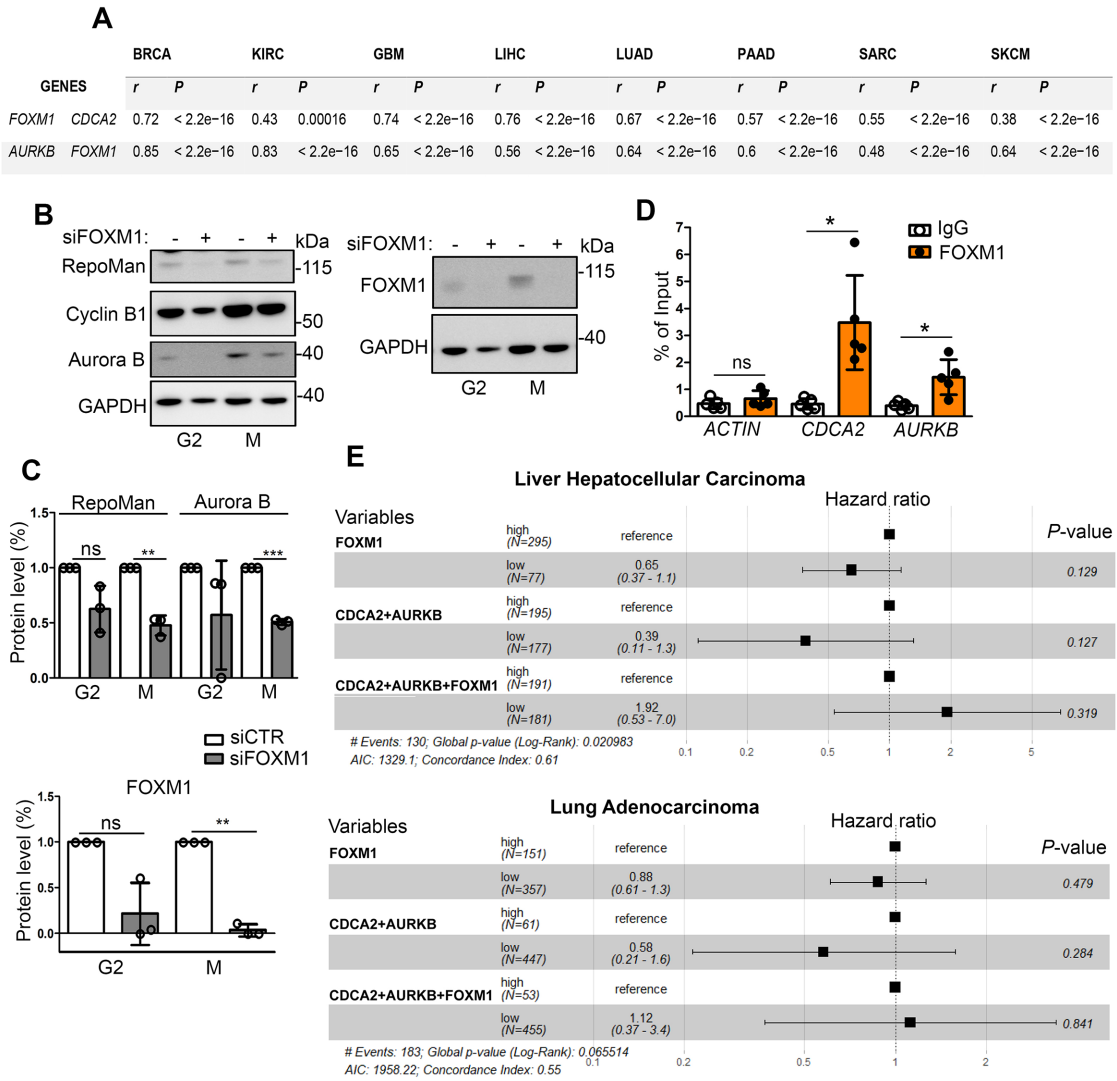

FIGURE 3: FOXM1 controls RepoMan and Aurora-B expression. (A) Summary of the Pearson's correlation coefficients (*r*) and *P* values for the indicated types of cancer, as defined in the legend of Figure 1. Transcript expression data (array z-score) of *CDCA2*, *AURKB*, and *FOXM1* were obtained from human cancer data sets in the cBioPortal database. (B) U2OS cells were arrested in G2 (thymidine block and RO3306) or in mitosis (thymidine block and nocodazole) before and after the knockdown of FOXM1. Cell lysates were analyzed by immunoblotting. (C) RepoMan, Aurora-B, and FOXM1 band intensities were quantified and normalized to GAPDH and to siCTR for each phase from three independent experiments. Ns, not significant; $^{**}P < 0.01$ and $^{***}P < 0.001$ in paired *t* test. (D) ChIP-qPCR assay for FOXM1 of the indicated genes in U2OS cells fixed after 10 h release from a G1/S arrest. Bars indicate the mean percentages ± SD of input precipitated with FOXM1 antibody or rabbit anti-mouse immunoglobulins (IgG). *ACTIN* was used as non-FOXM1 target gene. ChIP enrichments were calculated as a percentage of the total input signal (Ns, not significant; $^{*}P < 0.05$ in paired *t* test for five independent experiments). (E) Cox-proportional hazards model showing the hazard risk for the indicated variables in patients with liver hepatocellular carcinoma or lung adenocarcinoma. N, number of patients.

knockdown of CDH1. Quantification of mClover-RepoMan in single cells confirmed the stabilization of RepoMan at the mitotic exit in CDH1-depleted cells (Figure 4E and Supplemental Figure S4, E and F). Collectively, these findings identified RepoMan as a novel late-mitotic substrate of the APC/C-CDH1 complex.

CDH1 recruits APC/C substrates through interaction with degrons, in particular so-called destruction (D) and KEN boxes (He *et al.*, 2013). To identify degrons in RepoMan, we first used N-terminal deletion mutagenesis to map the RepoMan domain that mediates binding to CDH1 (Figure 4F). This analysis revealed that residues 403–550, and to some extent also residues 1–402, of RepoMan, are required for coprecipitation with endogenous CDH1 (Figure 4F). Internal deletions (Δ) in full-length RepoMan enabled us to map the key CDH1 binding domain more precisely to residues 441–472, which are conserved in mammals (Figure 4G). Using the APC/C degron depository (http://slim.ucd.ie/apc/index.php), we did not find a canonical D box or KEN box in residues 441–472, but identified residues 455–457 as a putative non-canonical KEN box. Indeed, when these residues were mutated to Alanine (LEN/AAA), RepoMan largely lost its ability to bind CDH1 (Figure 4H), indicating that they mediate the binding of RepoMan to CDH1. To validate the importance of this putative KEN box for RepoMan degradation, we compared the levels of EGFP-RepoMan WT, Δ441-472, and LEN/AAA in HEK293T cells before

and after the overexpression or knockdown of CDH1 (Figure 4, I–L). In contrast to RepoMan WT, the CDH1-binding mutants of RepoMan (Δ441-472 and LEN/AAA) were not significantly affected by the overexpression or knockdown of CDH1. We also noted that the in vivo ubiquitination of EGFP-RepoMan WT, triggered by the overexpression of CDH1 and His-tagged ubiquitin, was not detected with the LEN/AAA mutant (Supplemental Figure S4G). Collectively, these data demonstrated the functional relevance of the LEN motif for APC/C-CDH1-mediated degradation of RepoMan (Figure 4M). However, we cannot rule out that other motifs in the N-terminus (residues 1–402) of RepoMan somehow contribute to the stabilization of its interaction with CDH1 (Figure 4F).

FBXW7α contributes to the turnover of RepoMan in interphase

The proteasome inhibitor MG132 stabilized RepoMan in both asynchronous U2OS cells (Figure 2, G and H) and in cells that were arrested in G1/S (Supplemental Figure S5, A and B), indicating that RepoMan is also targeted for proteasomal degradation in interphase. As APC/C-CDH1 is inactivated in late G1 (Brandeis and Hunt, 1996; Cappell *et al.*, 2016), the down-regulation of RepoMan in G1/S likely involves another E3 ubiquitin ligase. SCF^{FBXW7} emerged as an attractive candidate as it targets many cell cycle-regulated proteins for degradation during interphase, including Aurora B (Teng *et al.*, 2012). The human *FBXW7* gene encodes three isoforms (α, β, and γ), which are targeted to distinct subcellular compartments (Welcker *et al.*, 2004). Since RepoMan is associated with chromatin during interphase we focused on the nuclear α-isoform of FBXW7. First, we verified that EGFP-RepoMan, but not EGFP-β-gal, interacted with ectopically expressed 3xFlag-tagged-FBXW7α (Figure 5A). Next, we found that recombinant His-tagged-RepoMan could be ubiquitinated by purified SCF^{FBXW7} complex in vitro (Figure 5B). In addition, we performed an in vivo ubiquitination assay in G1/S-arrested HEK293T cells (Supplemental Figure S5C). A dominant-negative fragment of CULLIN1 (DN-CUL1), which cannot recruit the E2 enzyme, completely abolished ubiquitination of EGFP-RepoMan. On the other hand, cotransfection of 3xFlag-tagged FBXW7α and Flag-WT-CULLIN1 resulted in increased levels of ubiquitinated EGFP-RepoMan. Moreover, the overexpression of FBXW7α reduced RepoMan abundance in G1/S-arrested U2OS cells while the depletion of FBXW7 in these conditions rescued RepoMan levels (Figure 5C). In contrast, the overexpression or knockdown of FBXW7 did not change *CDCA2* mRNA levels (Supplemental Figure S5, D and E).

Substrate recognition by FBXW7 involves the binding of its β-propeller-surface, formed by WD40 repeats, with a phosphodegron of its substrates (Koepp *et al.*, 2001). Consistent with this notion, we found that mutation of either of three residues of FBXW7α (R465, R479, R505) that are required for phosphodegron binding (Akhoondi *et al.*, 2007) reduced its interaction with EGFP-RepoMan in pull-down experiments (Figure 5D). In addition, treatment of EGFP-RepoMan traps with lambda phosphatase markedly reduced the RepoMan–FBXW7α interaction (Figure 5E), hinting at the existence of one or more RepoMan phosphodegrons that mediate its binding to FBXW7α. To further delineate the importance of RepoMan phosphorylation for FBXW7 recruitment, we examined the consequences of interfering with RepoMan phosphorylation. RepoMan contains 17 CDK consensus phosphorylation sites throughout its sequence and some of these are known to be phosphorylated in vivo (Olsen *et al.*, 2010; Vagnarelli *et al.*, 2011; Prévost *et al.*, 2013; Qian *et al.*, 2015) (Figure 5F). CDK inhibition with roscovitine reduced the RepoMan-FBXW7 interaction (Figure 5G), suggesting that CDK-mediated phosphorylation somehow promotes the RepoMan–FBXW7α interaction. Previous studies showed that residues 403–550 of RepoMan mediate binding of CDK/Cyclin complexes (Qian *et al.*, 2015). Therefore, we examined whether the internal deletion of this fragment (Δ400–550) affected the interaction between RepoMan and FBXW7. First, we confirmed a reduced interaction between RepoMan-Δ400-550 and endogenous CDK2 (Figure 5H). Second, RepoMan-Δ400–550 showed a reduced association with FBXW7 (Figure 5H) and was more stable in the presence of 3xFlag-tagged-FBXW7α as compared with RepoMan WT (Figure 5, I and J). In conclusion, these data suggested that the SCF^{FBXW7}-mediated degradation of RepoMan during interphase depends on the phosphorylation of one or more CDK sites (Figure 5K). Further studies are required to map the involved phosphodegron(s) of RepoMan.

A theoretical model of the co-regulation of RepoMan and Aurora B

To gain more insights into the significance of the co-regulation of RepoMan and Aurora B, we developed a theoretical model using well-established parts of the cell-cycle regulatory network. A sketch of the simplified regulatory network that we considered is shown in Figure 6A. It consists of two main interaction modules: one centered on CDK1-Cyclin B (the CDK1 module) and one focused on the CPC (the Aurora-B module). One intriguing observation is that both modules function very similarly in that they both include feedback mechanisms with regulatory kinases and phosphatases. In both cases there is positive feedback: CDK1-Cyclin B activates its activating phosphatase CDC25 (Hoffmann *et al.*, 1993), and Aurora B activates its activating kinase Haspin (Wang *et al.*, 2011). Likewise, the modules both contain double-negative feedback: CDK1-Cyclin B inhibits its inhibitory kinase WEE1 (Parker and Piwnica-Worms, 1992), and Aurora B restrains its inhibitory phosphatase PP1-RepoMan (Qian *et al.*, 2013). These types of interactions are known to generate so-called bistability, meaning that under the same conditions the substrate can find itself in a condition of either low phosphorylation or high phosphorylation (Ferrell, 2013; Gelens *et al.*, 2018) (see, e.g., Figure 6B, shaded area). This bistability is controlled differently in both modules. In the CDK1 module, Cyclin-B levels determine the total amount of the protein complex CDK1-Cyclin B (the abundance of the CDK1 kinase itself is constant; Figure 6, B and D). The phosphorylation state, which regulates the activity of CDK1-Cyclin B, is then controlled by feedback loops involving approximately constant amounts of CDC25 and WEE1 protein. Bistability in the CDK1 module was experimentally demonstrated independently by two groups (Pomerening *et al.*, 2003; Sha *et al.*, 2003). In the Aurora-B module, CDK1-Cyclin B drives localization of Aurora B to the centromeres (see *Introduction*) (Figure 6A). This can again lead to regions of bistability in Aurora B versus PP1-RepoMan activity at the chromosomes. Experimental evidence of bistability in Aurora-B activity generated through positive feedback was reported recently by Zaytsev *et al.* (2016). In contrast to the CDK1 module, however, the total abundance of the Aurora-B and RepoMan protein level changes throughout the cell cycle (Figure 2). We found that an increase in the concentration of Aurora B and RepoMan leads to bistability in a wider range of CDK1 activities (Figure 6C). Moreover, the bistable region as a whole shifted to lower CDK1 activities. As Aurora B and RepoMan abundances increase, less active CDK1 is needed to flip the balance between Aurora B and RepoMan. Moreover, once this switch is made, high abundances of Aurora B and RepoMan ensure that Aurora B remains dominant over PP1-RepoMan, making the system more robust to stochastic changes in the environment.

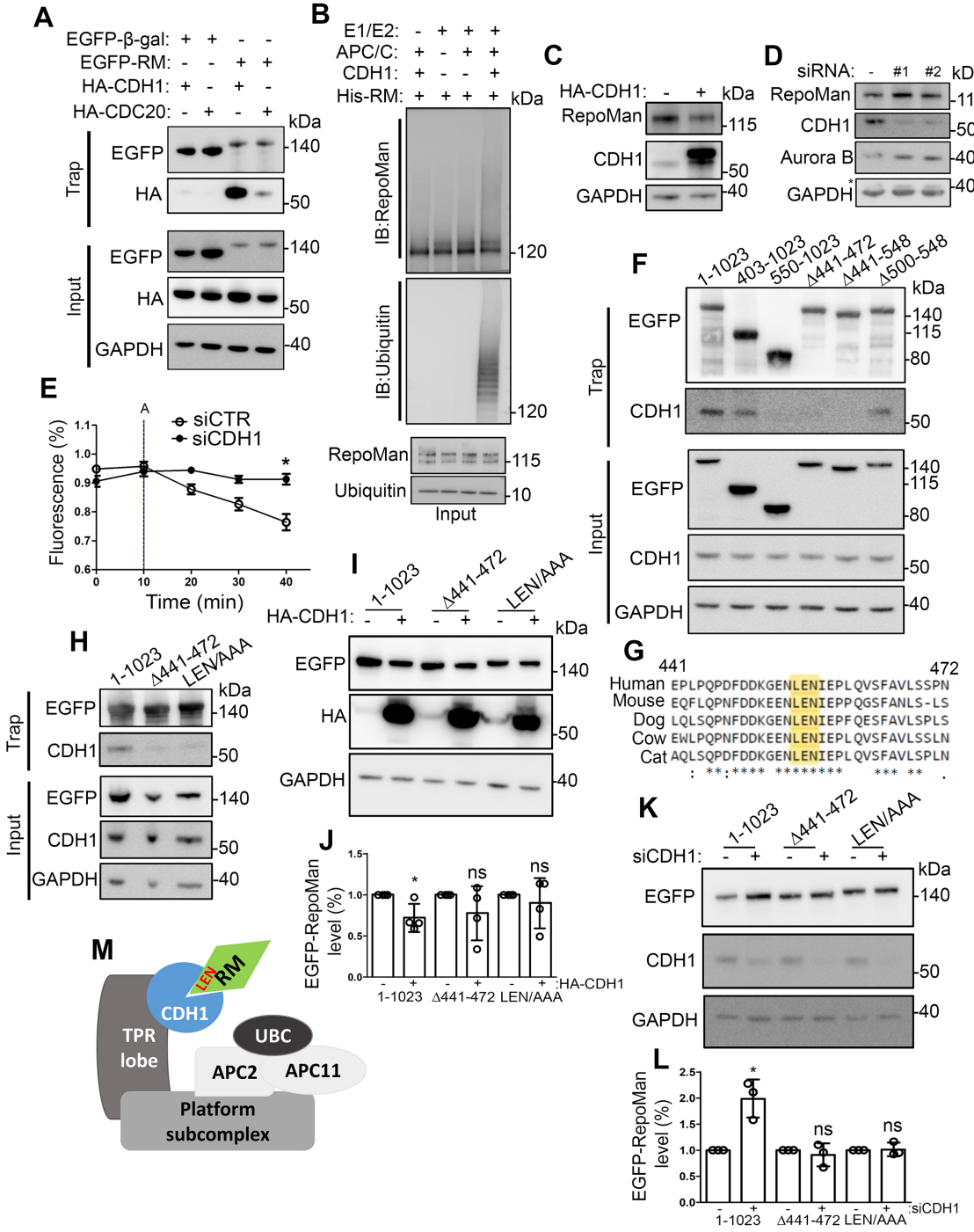

FIGURE 4: APC/C-CDH1 targets RepoMan for proteasomal degradation at the mitotic exit. (A) Lysates and EGFP traps from nonsynchronized HEK293T cells coexpressing EGFP-tagged β-gal or EGFP-RepoMan-S893D (EGFP-RM) and either HA-CDH1 or HA-CDC20 were processed for immunoblotting. (B) In vitro ubiquitination assay of His-tagged RepoMan using purified human APC/C and CDH1. The reaction was performed for 45 min at 23°C in the absence (–) or the presence (+) of the indicated components. E1, UBE1; E2, UBCH10. RepoMan-ubiquitination was detected by immunoblotting (IB) for both RepoMan and ubiquitin, as indicated. (C) U2OS cells were transfected or not with HA-CDH1 before immunoblotting of the lysates. (D) U2OS cells were transfected for 48 h with control (siCTR) or either of two different siRNAs against CDH1 before immunoblotting of the lysates (*the residual band is Aurora B after reprobe of the blot for GAPDH). (E) Degradation curves of mClover-RepoMan after depletion of CDH1 in HeLa cells obtained by quantifying the levels of mClover-RepoMan from ≥10 cells per condition per experiment from three replicates. The intensity of fluorescence was measured at 0, 10, 20, 30, and 40 min from the beginning of metaphase, and the normalized values were plotted against time. A, anaphase; *$P < 0.05$ in paired t test. See also Supplemental Figure S4, E and F. (F) Immunoblot analysis of EGFP traps of lysates from nonsynchronized HEK293T cells expressing EGFP-tagged RepoMan-S893D or the indicated corresponding deletion mutants. (G) Conservation of residues 441–472 of RepoMan in mammals using Clustal Omega program formatting. (H) Effect of the deletion of residues 441–472

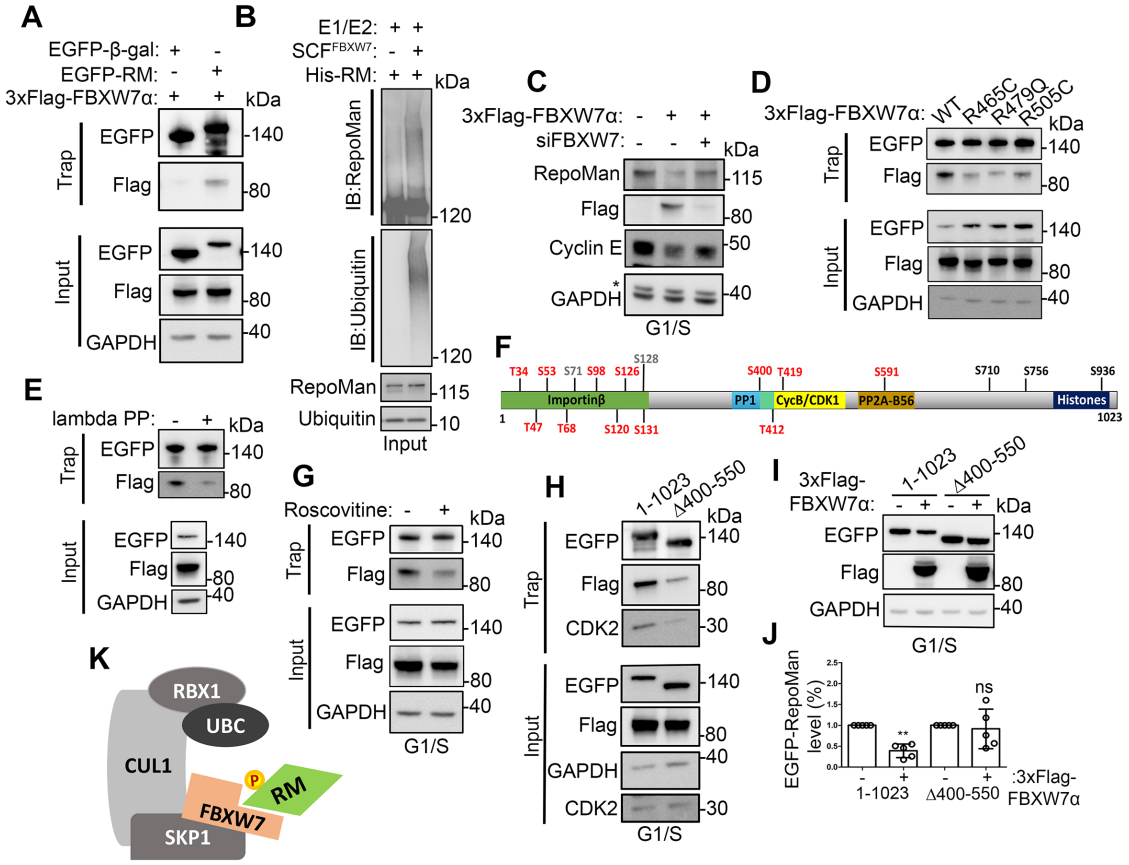

FIGURE 5: The SCF^{FBXW7} complex promotes RepoMan degradation in interphase. (A) EGFP traps of lysates from nonsynchronized HEK293T cells coexpressing 3xFlag-FBXW7α and either EGFP-tagged β-gal or EGFP-RepoMan-S893D were processed for immunoblotting. (B) In vitro ubiquitination of His-RepoMan by recombinant SCF^{FBXW7}. The reaction was performed in the presence of E1 (UBE1) and E2 (UBCH3) at 30°C for 90 min. RepoMan-ubiquitination was detected by immunoblotting (IB) for both RepoMan and ubiquitin, as indicated. (C) Immunoblot analysis of lysates from U2OS cells arrested in G1/S phase nontransfected or transfected with 3xFlag-FBXW7α and siCTR (–) or 3xFlag-FBXW7α and siFBXW7 (+). *Residual band after reprobe of the blot for GAPDH. (D) Immunoblot analysis of EGFP traps from nonsynchronized HEK293T cells expressing EGFP-RepoMan-S893D and one of the indicated mutants of FBXW7α. (E) EGFP-RepoMan-S893D traps from nonsynchronized HEK293T cells were preincubated with buffer or lambda phosphatase (lambda PP) and examined for retained ectopically expressed FBXW7α. (F) Schematic representation of the predicted and established CDK phosphorylation sites of human RepoMan. Red, established phosphorylation site (Dephoure *et al.*, 2008; Olsen *et al.*, 2010; Vagnarelli *et al.*, 2011; Prévost *et al.*, 2013; Qian *et al.*, 2015). Black, CDK phosphorylation sites, as determined by mass spectrometry (Wu *et al.*, 2018); gray, CDK phospho-sites predicted by NetPhos 3.1 (Blom *et al.*, 2004). (G) HEK293T cells that transiently expressed EGFP-RepoMan-S893D and 3xFlag-FBXW7α were arrested in G1/S with a single thymidine block and treated for 4 h with DMSO or 20 μM roscovitine to examine the effect on the retention of FBXW7α by EGFP-traps. (H) Effect of the deletion of residues 400–550 (Δ400–550) on the binding of ectopically expressed 3x-Flag-FBXW7α and endogenous CDK2 to EGFP-RepoMan-S893D in G1/S HEK293T cells. (I) Immunoblot analysis of lysates from G1/S HEK293T cells expressing EGFP-tagged RepoMan-S893D or Δ400-550 in the absence (–) or presence (+) of 3x-Flag-FBXW7α. (J) Relative abundance of EGFP-RepoMan levels from five independent experiments normalized to GAPDH and to the control (no transfection of 3xFlag-FBXW7α). Ns, not significant; ***P* value < 0.01 in paired *t* test. (K) Cartoon of the SCF^{FBXW7} complex associated with phosphorylated RepoMan (RM). Adapted from Crusio *et al.* (2010). SKP1, S-phase kinase-associated protein 1; CUL1, Cullin-1; RBX1, E3 ubiquitin-protein ligase RBX1.

(Δ441–472) or alanine mutation of residues 455–457 (LEN/AAA) on the binding of CDH1 to EGFP-RepoMan-S893D in HEK293T lysates. (I) Immunoblot analysis of lysates from nonsynchronized HEK293T cells expressing EGFP-tagged RepoMan-S893D or the indicated mutants in the absence (–) or the presence (+) of HA-CDH1. (J) Relative abundance of EGFP-RepoMan levels from four independent experiments normalized to GAPDH and to the control (no transfection of HA-CDH1). Ns, not significant; **P* < 0.05 in paired *t* test. (K) Immunoblot analysis of lysates from nonsynchronized HEK293T cells expressing EGFP-tagged RepoMan-S893D or the indicated mutants after transfection with siCTR (–) or siCDH1 (+). (L) Quantification of EGFP-RepoMan levels from three independent experiments normalized to GAPDH and to the control (siCTR). Ns, not significant; **P* < 0.05 in paired *t* test. Since the expression level of the RepoMan (mutants) showed small differences, we compared each RepoMan variant with its own control (no HA-CDH1 or siCTR) for quantifications shown in J and L. (M) Cartoon of the APC/C associated with the cofactor CDH1 (adapted from Sivakumar and Gorbsky, 2015). RM, RepoMan; TPR, tetratricopeptide repeat; UBC, ubiquitin-conjugating enzymes.

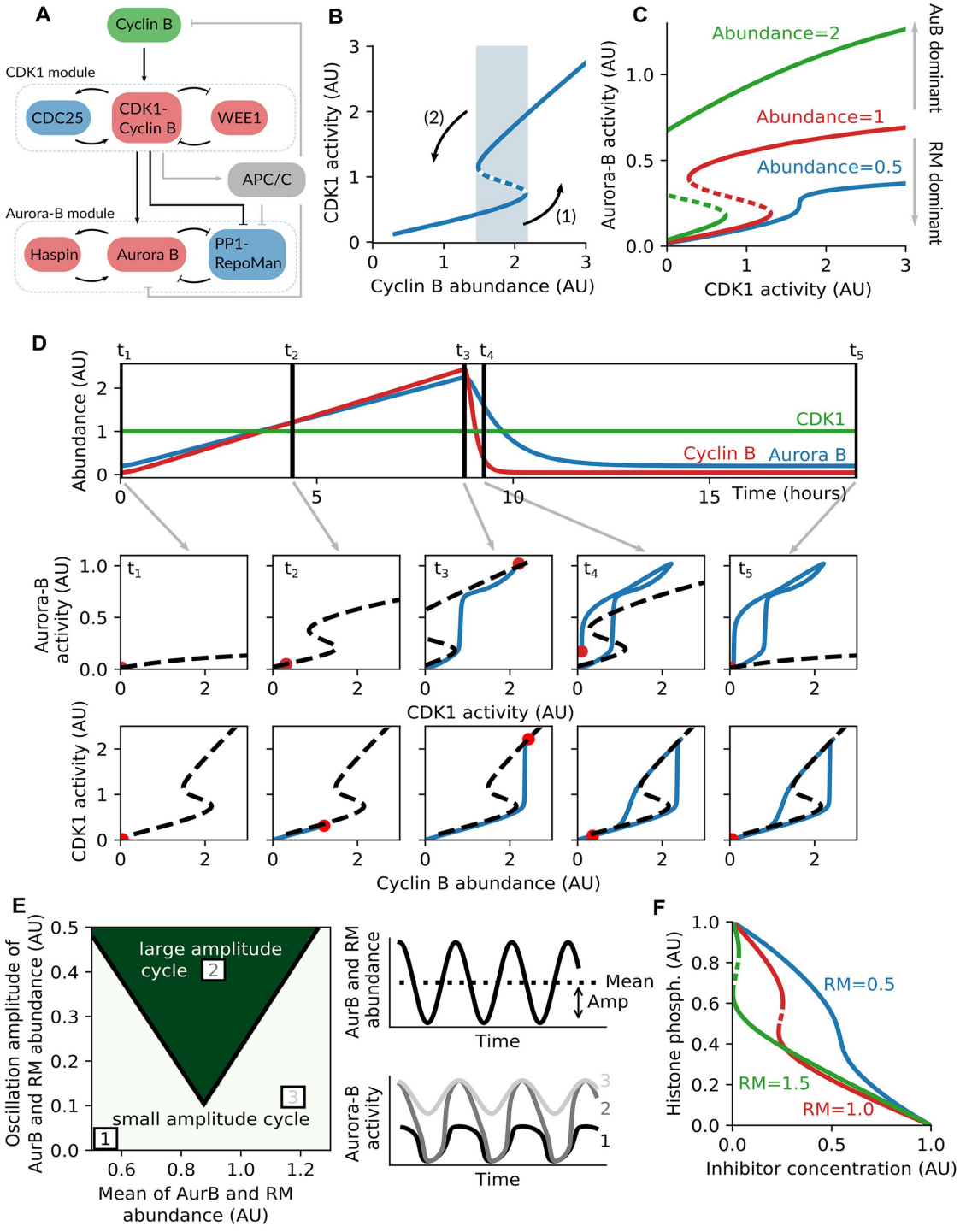

FIGURE 6: A theoretical model captures the co-regulation of RepoMan and Aurora B. (A) Diagram showing protein interactions in a simplified cell-cycle regulatory network. (B) The CDK1 module generates a bistable switch in steady state. For low and high levels of Cyclin B, only the corresponding low or high activities of CDK1 exists, but for intermediate values (shaded zone), CDK1 can be either in a state of low activity or high activity. (C) The Aurora-B module can also generate a bistable switch of Aurora-B activity in response to CDK1 activity. The shape of the curve is modified by changing abundances of RepoMan and Aurora-B. (D) Time series simulation of the coupled modules in A during one cell cycle. The timing is determined by production and degradation of the different proteins via ubiquitination by ligases such as APC/C and SCF^{FBXW7}. First row: levels of Aurora-B abundance, CDK1 abundance, and Cyclin B abundance over time. Second row: response of Aurora-B activity to CDK1 activity (dashed line). The blue line traces the current levels of CDK1 activity and Aurora-B activity (red dot). In particular, it shows how the activities change differently when CDK1 activity increases and decreases. Note that, due to varying levels of total Aurora B, the response curve also changes. Third row: response of CDK1 activity to Cyclin B abundance (dashed curve) and current levels (red dot). Since total CDK1 remains constant, the response curve does not change in time. (E) Large or small amplitude

Next, we set out to expand our theoretical model by taking into account the temporal regulation of all proteins involved, as shown in Figure 6A. First, the CDK1 module is controlled in time by changes in the abundance of Cyclin B. Cyclin B accumulates throughout interphase, which eventually triggers activation of the CDK-Cyclin B complex (see (1) in Figure 6B). Active CDK1-Cyclin B then activates the APC/C complex, which tags Cyclin B for degradation by the proteasome via ubiquitination, and thus eventually leads to the deactivation of CDK1-Cyclin B (see (2) in Figure 6B). Altogether, this leads to regular oscillations in Cyclin-B abundance and CDK1 activity as illustrated in Figure 6D. Second, these periodic changes in CDK1-Cyclin B and APC/C activity drive the temporal dynamics of the Aurora-B module. However, in contrast to the CDK1 module, the activity of Aurora B and PP1-RepoMan are no longer determined by a static bistable switch. Instead, due to the fact that Aurora B and RepoMan abundances continuously change, the bistable switch in the Aurora-B module dynamically changes as well (see five snapshots t_1–t_5 in Figure 6D). As Aurora B and RepoMan abundances increase with time (panels t_1–t_3), the threshold to flip the switch is reduced, facilitating a sudden increase in Aurora B versus PP1-RepoMan activity as this threshold is passed.

We then wondered whether dynamically changing such a bistable switch in time would have obvious advantages in terms of robustness of the oscillations in Aurora-B activity. Therefore, in Figure 6E and Supplemental Figure S6, we changed the oscillation amplitude and mean of the Aurora B and PP1-RepoMan abundances and plotted for which of these parameter values the system showed oscillations in Aurora-B activity of sufficient amplitude (for details see *Materials and Methods*). This analysis revealed that increasingly modulating the bistable switch leads to robust oscillations of Aurora-B activity (see dark green region in Figure 6E). We speculate that this type of dynamic regulation is a general feature in biology. Indeed, in recent work by Vergassola *et al.* (2018), the authors have shown experimentally that a similar time dependence of the well-characterized CDK1 switch exists in *Drosophila* embryos, and they found that this type of regulation provides a unique mechanism to generate a wave-like spreading of CDK1 activity that is faster than in the absence of such dynamic regulation (Vergassola *et al.*, 2018).

On the basis of our model, we wondered whether we could exploit the theoretically observed changes in the regions of bistability in response to changing Aurora B and RepoMan abundances (Figure 6C) for improved cancer therapy, focusing on Aurora-B inhibitors (Borisa and Bhatt, 2017). We examined how the phosphorylation of histone H3, a well-established Aurora-B substrate, changed with increasing inhibitor concentrations and repeated this analysis for increasing abundances of RepoMan, thus increasing the RepoMan:Aurora-B ratio. This analysis, which implements an increase in inhibitor as an effective decrease of Aurora B abundance, shows that increasing the inhibitor decreases the width of the bistable switch, which eventually triggers the system to transition from a high to a low Aurora-B activity state. Increasing RepoMan abundance additionally decreases the width of the bistable switch, thus lowering the amount of Aurora-B inhibitor that is required to significantly decrease the amount of histone H3 phosphorylation (Figure 6F).

The RepoMan:Aurora-B balance determines the sensitivity to Aurora-B inhibitors

To experimentally validate our prediction that cancer cells are more sensitive to Aurora-B inhibitors at high RepoMan levels, we first examined how the sensitivity of monastrol-arrested HeLa cells to the Aurora-B inhibitor hesperadin (Hauf *et al.*, 2003) is affected by the overexpression of mClover-tagged RepoMan. As a readout for Aurora-B activity, we quantified histone H3 phosphorylation at Ser10. The expression of RepoMan per se did not significantly affect H3S10 phosphorylation (Figure 7, A and B), but Aurora B inhibition reduced the mitotic phosphorylation at H3S10, as expected. The inhibition of Aurora B was also confirmed by increased association of RepoMan with the chromatin (Figure 7A), as previously observed (Qian *et al.*, 2013). Strikingly, the sensitivity to hesperadin was considerably increased following the overexpression of RepoMan, as predicted by our model (Figure 6F). Likewise, cell proliferation was not affected by the mere overexpression of RepoMan but was reduced when Aurora B was simultaneously inhibited with low concentrations of hesperadin (Figure 7C) or the structurally unrelated AZD1152 (Figure 7D). Finally, we explored how the expression of *CDCA2* and *AURKB* affects the sensitivity of CCLE cancer cell lines to Aurora-B inhibitors using data from the Genomics of Drug Sensitivity in Cancer (GDSC) database (Yang *et al.*, 2013), which is regularly updated. Cells with a high expression of either *AURKB* or *CDCA2* were generally more sensitive to the Aurora-B inhibitor ZM447439, as compared with cells that have low transcript levels (Figure 7E). An even higher sensitivity was noted for tumor cells that overexpressed both *AURKB* and *CDCA2* (Figure 7F). Thus, the co-overexpression of *CDCA2* and *AURKB* sensitized cancer cells to Aurora-B inhibitors. Finally, we found that the *CDCA2/AURKB* overexpressing cell lines had the highest level of chromosomal instability (CIN), as indicated by the CIN70 signature (Supplemental Figure S7A) (Carter *et al.*, 2006). Importantly, a higher CIN level in this subset of cell lines was associated with even greater ZM447439 sensitivity, as compared with these with lower CIN (Supplemental Figure S7B).

DISCUSSION

Precise regulation of reversible protein phosphorylation requires a strict control of the involved kinase/phosphatase pair(s). However, it is largely unknown how the balance between counteracting kinases and phosphatases is maintained. Here we demonstrated that the RepoMan and Aurora-B transcript and protein levels co-oscillate during the cell cycle (Figure 2). Such co-oscillation relies on at least three shared pathways. First, *CDCA2* and *AURKB* are a common target for the transcription factor FOXM1 (Figure 3; Wang *et al.*, 2005; Bonet *et al.*, 2012; Fischer *et al.*, 2016b). Second, a previous study revealed that the decay of *CDCA2* and *AURKB* transcripts is controlled by the CCR4-NOT deadenylation pathway (Rambout *et al.*, 2016). Third, the proteasomal degradation of both RepoMan and Aurora B depends on the ubiquitin ligases APC/C-CDH1 and SCF^{FBXW7} at the mitotic exit and during interphase, respectively (Figures 4 and 5; Stewart and Fang, 2005; Teng *et al.*, 2012). Hence, Aurora B and RepoMan are co-regulated on at least three levels, namely transcription, mRNA decay, and protein degradation (Figure 8A). FOXM1 is frequently up-regulated in cancer

oscillations in Aurora-B activity (see profiles 1-2-3) can be obtained in response to periodic changes (with varying mean and amplitude) of the total abundance of both Aurora B and RepoMan. For details, see *Materials and Methods* and Supplemental Figure S6. (F) By increasing RepoMan abundance, the sensitivity of Aurora B to inhibitors is increased.

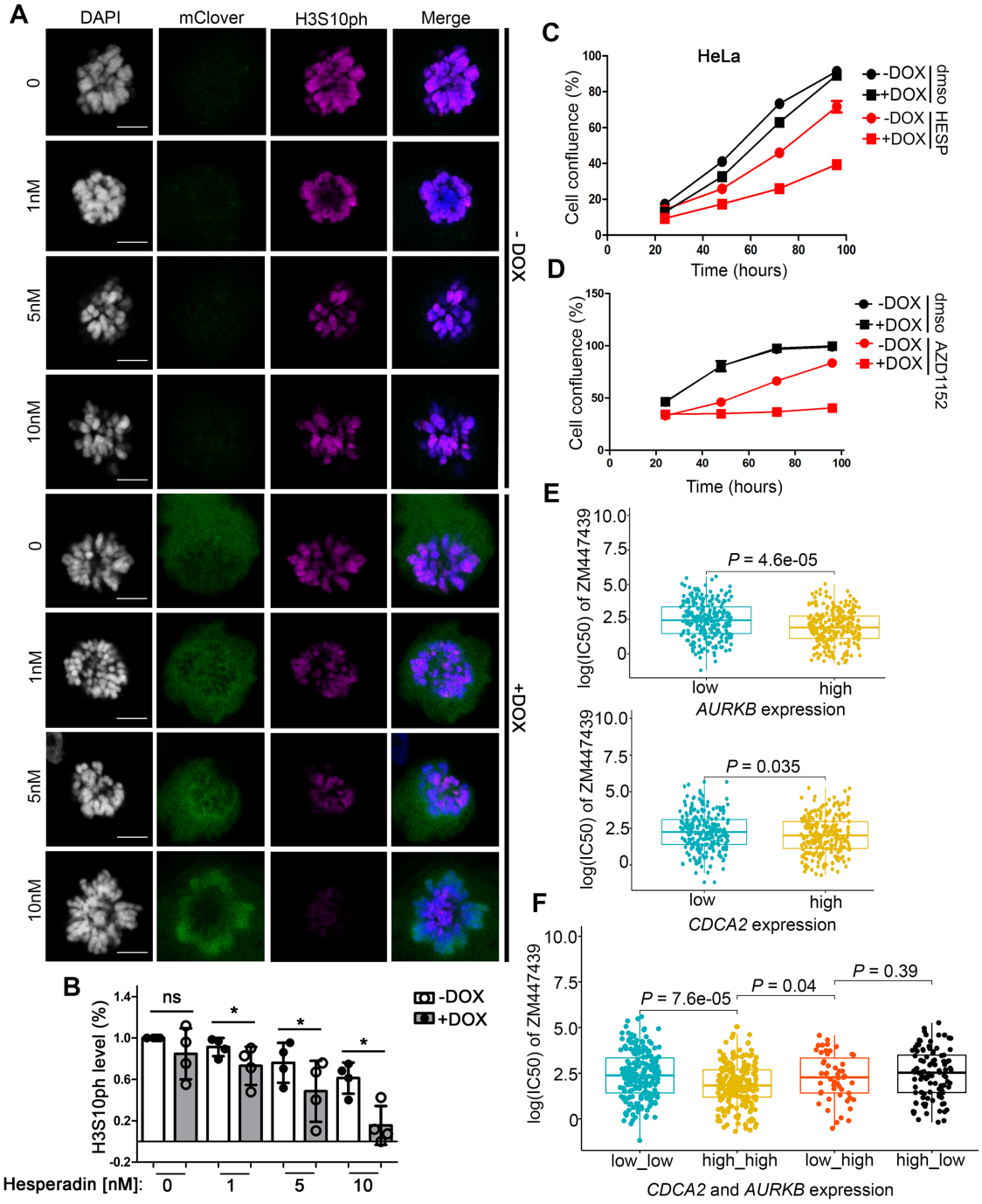

FIGURE 7: Overexpression of RepoMan sensitizes cancer cells to Aurora-B inhibitors. (A) Monastrol-arrested HeLa Flp-In T-REx cells were treated for 1 h with the indicated concentrations of hesperadin before (-DOX) and after induction (+DOX) of mClover-tagged RepoMan. Cells were fixed and stained. (B) Quantification of the H3S10ph/DNA ratio in A. The graph shows the mean percentage ± SD from four independent experiments (≥25 cells for each condition per experiment). *$P < 0.05$ in paired *t* test. (C) Percentage of confluence over time of HeLa Flp-In T-REx cells before and after induction with Dox and treated with either DMSO or 20 nM hesperadin. The growth curves are representative of three experiments and were obtained from confluence measurements acquired at 2 h intervals using IncuCyte software. (D) Same as C but after treatment with DMSO or 15 nM AZD1152. (E) ZM447439 sensitivity (IC50) prediction from cancer cell lines (CCLE) when comparing low and high *AURKB* or *CDCA2* expression. Differences in median log(IC50) across the subgroups were evaluated with the Wilcoxon–Mann–Whitney Test. (F) The co–up-regulation of *CDCA2* and *AURKB* (high_high) significantly reduces the log(IC50) of ZM447439 in cancer cell lines (CCLE). Differences in median log(IC50) across the subgroups were evaluated with the Wilcoxon–Mann–Whitney Test.

(Raychaudhuri and Park, 2011) and ubiquitin-mediated protein degradation is also often deregulated in cancers (Nakayama and Nakayama, 2006). For example, the tumor suppressor gene *FBXW7* is commonly mutated and multiple oncogenic pathways are associated with the inactivation of CDH1 (Lehman *et al.*, 2006; Davis *et al.*, 2014; Wan *et al.*, 2017). Hence, the dysregulation of shared

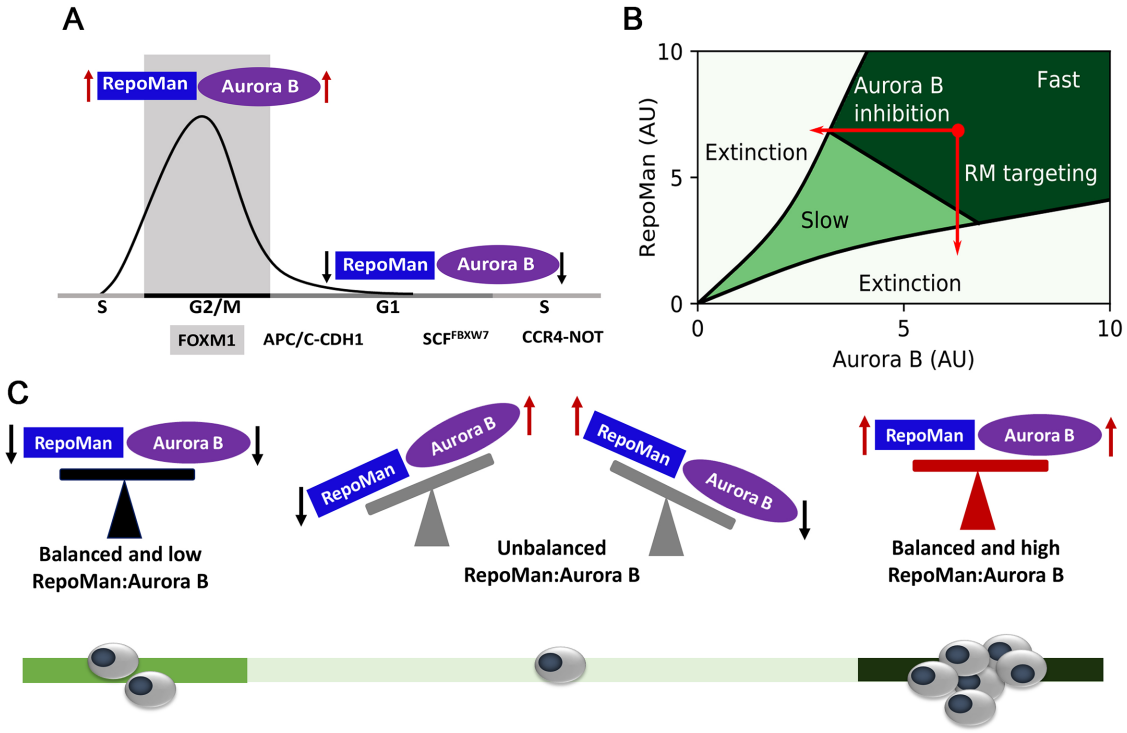

FIGURE 8: Model for the co-regulation of RepoMan and Aurora B in cancer cells. (A) RepoMan and Aurora B are co-regulated at multiple levels during the cell cycle. Gray zone: the two counteracting enzymes have maximal expression in G2/M in a FOXM1-dependent manner; white zone: during mitotic exit and early G1 the ubiquitin ligase APC/C-CDH1 down-regulates RepoMan and Aurora B; during interphase (likely G1/S transition) SCF^{FBXW7} is involved in the proteolytic turnover of RepoMan and Aurora B; *CDCA2* and *AURKB* transcripts are down-regulated in S phase by a mRNA decay pathway involving ERG-CCR4-NOT. (B) Phenomenological model that captures how the growth rate of cancer cells changes with varying concentrations of RepoMan and Aurora B, as well as their ratio. (C) Hypothetical model for RepoMan and Aurora-B co–up-regulation in cancer cells based on B. Cancer cells (gray ovals) with a low and balanced ratio of RepoMan and Aurora B (black scale) grow slowly (light green bar), as compared with tumor cells with high and balanced RepoMan:Aurora-B ratio (red scale and dark green bar). Unbalanced levels of the two proteins (gray scale) is disadvantageous for cell proliferation (pale green bar).

(post)transcriptional control mechanisms can account for the co-overexpression of RepoMan and Aurora B in many cancers (Figures 1 and 2A), which is often associated with enhanced tumor progression (Figure 1). However, as the level of other cell cycle-regulated proteins is also increased in tumors, it remains to be determined to which extent the up-regulation of RepoMan and Aurora B contributes to tumor progression.

Aneuploidy is a double-edged sword for cancers: a low level of aneuploidy fuels tumor progression by increasing genetic instability, while a high level of aneuploidy is lethal (Sansregret *et al.*, 2018). It has been shown that the down-regulation of RepoMan or Aurora B, but also the overexpression of Aurora B, often results in chromosome segregation errors, a well-established cause of aneuploidy (Ota *et al.*, 2002; Hauf *et al.*, 2003; Cimini *et al.*, 2006; Trinkle-Mulcahy *et al.*, 2006; Vagnarelli *et al.*, 2006; Wurzenberger *et al.*, 2012; Britigan *et al.*, 2014; González-Loyola *et al.*, 2015; Qian *et al.*, 2015). We speculate that the co–up-regulation of RepoMan and Aurora B in cancer cells maintains their balance to limit aneuploidy to levels that are beneficial for tumor progression. Furthermore, a sustained RepoMan:Aurora B balance may prevent excessive or prolonged SAC activation caused by Aurora-B induced disruption of erroneous KT-MT interactions. But why is the co–up-regulation of RepoMan and Aurora B in cancer associated with poor patient survival, even if their balance is maintained? Considerable evidence from the literature suggests that high levels of RepoMan and Aurora B are beneficial for cancer cells because they independently reduce the threshold for checkpoint-induced cell-cycle arrest during interphase. Indeed, RepoMan overexpression allows cell-cycle progression in the presence of DNA double-strand breaks. This is explained by the dephosphorylation and inactivation of the DNA damage-activated protein kinase ATM by PP1-RepoMan, thereby preventing the stabilization of p53 and expression of the CDK inhibitor $p21^{Cip1}$ (Peng *et al.*, 2010; Uchida *et al.*, 2013). RepoMan also promotes the progression through G0/G1, as suggested by the reduced levels of CDK4, CDK6, Cyclin D1, and Cyclin E after the knockdown of RepoMan, but the underlying mechanism is not known (Uchida *et al.*, 2013). Aurora B promotes cell-cycle progression through direct phosphorylation and inactivation of p53 (Gully *et al.*, 2012). In addition, Aurora B impairs the DNA damage response, but the relevant substrate remains to be identified (González-Loyola *et al.*, 2015). Collectively, the available data suggest that cancer cells maintain their RepoMan:Aurora B balance to limit SAC signaling and aneuploidy to nonlethal levels; at the same time, the increased expression levels of RepoMan and Aurora B independently promote cancer cell proliferation by overruling checkpoint-mediated cell-cycle arrest.

To better understand the effect of the co-oscillation of Aurora B and RepoMan, we studied a mathematical model of the system which includes production, degradation, and various feedback loops. One possible function of Aurora B and RepoMan being cell

cycle regulated is the fact that more robust transitions between low and high activity states are possible when various positive feedback loops are combined with changing abundances. The modeling also predicted that an increased level of RepoMan sensitizes cancer cells to Aurora-B inhibitors (Figure 6F) due to the complex interplay between Aurora-B and RepoMan signaling. This unexpected outcome was subsequently validated for two Aurora-B inhibitors in cells that express distinct levels of Aurora B and RepoMan and by analysis of their effects on cancer cell lines in the publicly available GDSC data set (Figure 7, E and F). It remains to be examined whether an increased sensitivity to Aurora-B inhibitors at high RepoMan levels also applies to a (pre)clinical setting. If so, the RepoMan expression level could possibly be used to identify patients that benefit most from an Aurora-B inhibitor-based therapy.

To more clearly illustrate how tumor growth could depend on the concentration and balance of RepoMan and Aurora B, we developed a simple model to mimic tumor growth (Figure 8B). This theoretical model incorporates an increasing growth rate of cancer cells when RepoMan and/or Aurora B are overexpressed and suppress cell-cycle checkpoints more strongly. This assumption is consistent with data from the literature (see *Introduction*) and the finding that the up-regulation of RepoMan and/or Aurora B correlates with tumor progression (Figure 1). Our model also hypothesizes that the probability of cancer cells to accumulate a lethal amount of aneuploidy increases with an increasing imbalance between Aurora B and RepoMan, consistent with available data (Ota *et al.*, 2002; Hauf *et al.*, 2003; Cimini *et al.*, 2006; Britigan *et al.*, 2014; González-Loyola *et al.*, 2015). Using these two basic assumptions, the theoretical model shows the existence of three qualitatively different regions: a slowly growing tumor, a rapidly growing tumor, and tumor extinction (Figure 8B). Rapid tumor growth is seen in the region where Aurora B and RepoMan are both overexpressed, while maintaining a balance between their activities. However, when this balance is disturbed beyond a critical threshold, the probability of cell death overcomes the division rate of the cells in the population and the tumor gets extinct. This fast-growth area is likely more vulnerable to RepoMan:Aurora B imbalance induced by an Aurora-B inhibitor (Figure 8B). However, pushing cancer cells into the extinction area by targeting RepoMan seems a similarly attractive option worth future exploration.

In conclusion, we have shown here that RepoMan and Aurora B are regulated by the same (post)transcriptional mechanisms, accounting for their co-oscillation during the cell cycle and co–up-regulation in various cancers. We propose that the co–up-regulation of RepoMan and Aurora B is beneficial for cancer cells because it limits aneuploidy and reduces checkpoint-induced cell-cycle arrest. Unexpectedly, RepoMan emerged from our studies as a sensitizer for Aurora-B inhibitors, which can possibly be exploited therapeutically.

MATERIALS AND METHODS

DNA plasmids and RNA interference

The siRNA-resistant EGFP-RepoMan construct was previously described (Qian *et al.*, 2015). HA-tagged expression vectors for human CDH1 and CDC20 were purchased from Addgene (HA-CDH1 Plasmid #11596; HA-CDC20 Plasmid #11594). The FBXW7α cDNA (purchased from PlasmID, Harvard Medical School, Boston, MA) was cloned into the 3xFlag-C1-vector with the NEBuilder method (NEBuilder High-Fidelity Master Mix) to generate 3xFlag-FBXW7α. The NEBuilder method was also adopted for the generation of EGFP-RepoMan, HA-CDH1, and 3xFlag-FBXW7α mutants. His-tagged ubiquitin plasmid was kindly provided by Dario R. Alessi (University of Dundee, UK). pcDNA3-DN-hCUL1-FLAG (Addgene plasmid #15818) was a gift from Wade Harper (Harvard Medical School); pCMV6-CUL1-Flag was purchased from Origene. Duplexes of siRNA oligos were ordered in the format of Dicer siRNA (Integrated DNA Technologies), according to the manufacturer's protocol. The sequences of the siRNAs (5′→3′) were as follows: luciferase siRNA as a control (siCTR): UAAGGCUAUGAAGAGAUAC; CDH1 siRNA 1: AUGAGAAGUCUCCCAGUCAG; CDH1 siRNA 2: ACGAUGUGUCUCCCUACUC; FBXW7 siRNA: CACAAAGCTGGTGTGTGCA. Duplexes of siRNA against FOXM1 (GGACCACUUUCCCUACUUUdTdT) were obtained from Dharmacon.

Antibodies

Antibodies against ACA (HCT-0100, ImmunoVision, 1:5000), Aurora B (611082, BD Transduction Laboratories, WB: 1:1000, IF: 1:250), CDH1 (CC43, Millipore, 1:500), Cyclin B1 (554177, BD Pharmingen, 1:5000), EGFP (sc-9996, Santa Cruz, 1:2000), Flag (F1804, Sigma-Aldrich, 1:1000), FOXM1 (sc-500, Santa Cruz, 1:500 for WB; GTX-102170, GeneTex, 1:250 for ChIP), GAPDH (2118, Cell Signaling, 1:5000), HA (home-made, WB: 1:5000), ubiquitin-HRP (AUB01, Cytoskeleton, 1:1000), H3S10ph (9706, Cell Signaling for IF, 1:1000; 06-570, Upstate-Merck, for WB, 1:1000), and RepoMan (HPA030049, Sigma, WB: 1:1000, IF: 1:300) were obtained from the indicated sources. For detection of His-tagged ubiquitin in Supplemental Figures S4G and 5C, the PVDF membrane was incubated with HisProbe-HRP Conjugate (15165, Thermo Scientific, 1: 2500). Secondary HRP–conjugated antibodies were purchased from Dako (Heverlee, Belgium). Secondary Alexa 488, 555, and 633 antibodies were obtained from Invitrogen (Carlsbad, CA).

Cell culture and transfections

HEK293T and U2OS were purchased from the American Type Culture Collection. HeLa and WI-38 were obtained from ECACC. RPE-1 were received from Susanne Lens (University Medical Center, Utrecht). A549 cells were obtained from Ines Royaux (Janssen Pharmaceutica, Beerse). HeLa and Flp-In T-REx HeLa cells (see below) were authenticated by STR profiling. None of the cell lines used here are found in the database of commonly misidentified cell lines that is maintained by ICLAC and NCBI Biosample and all were regularly screened for mycoplasma infection. HEK293T cells were cultured in high-glucose DMEM, supplemented with 10% fetal calf serum (FCS). HeLa and U2OS cells were cultured in low-glucose DMEM, supplemented with 10% FCS. RPE-1 cells were cultured in DMEM:F12 with 10% FCS. WI-38 cells were cultured in low-glucose DMEM, supplemented with 10% FCS and 1% NEAA; A549 cells were cultured in Ham's F12 Nutrient Medium (Ham's F12), supplemented with 2 mM L-glutamine and 10% FCS. All media contained penicillin and streptomycin. Transfection with plasmid DNA was carried out with jetPRIME (Polyplus Transfection) transfection Reagent. The siRNA transfections or cotransfection of plasmid DNA and siRNA were performed using jetPRIME transfection reagent. Flp-In T-REx HeLa cells used for generating stable doxycycline (Dox)-inducible cell lines were a gift of Stephen Taylor (Manchester University, UK). Flp-In T-REx HeLa host cell lines were maintained in DMEM with 10% tetracycline-free fetal bovine serum (FBS) supplemented with 50 µg/ml Zeocin. The siRNA-resistant construct encoding mClover-RepoMan was cloned into the pCDNA5/FRT/TO vector (Invitrogen). HeLa Flp-In cells stably expressing a Dox-inducible construct of mClover-RepoMan were generated from the HeLa Flp-In host cell line by transfection with the pCDNA5/FRT/TO vector and pOG44 (Invitrogen) and cultured in the same medium but containing 200 µg/ml hygromycin and 4 µg/ml blasticidin. Transgene expression was induced with

100 ng/ml Dox (Sigma-Aldrich) for at least 24 h. Unless indicated otherwise, a prometaphase arrest was induced by culturing cells consecutively for 24 h with 2 mM thymidine, 2 h without thymidine, and 14 h with 100 ng/ml nocodazole. The prometaphase-arrested cells were harvested by shake-off. For the G1/S release experiments (U2OS cells), we first induced a double-thymidine arrest (2 mM thymidine for 18 h, 9 h release, 2 mM thymidine for 16 h). Then, the cells were harvested at the indicated time points after washout with phosphate-buffered saline (PBS).

Immunoblot and immunoprecipitation

For immunoblotting, cell lysates were prepared in lysis buffer containing 50 mM Tris-HCl at pH 7.4, 10% (vol/vol) glycerol, 0.5% Triton X-100, 150 or 300 mM NaCl, 0.5 mM phenylmethylsulfonyl fluoride (PMSF), 5 µM leupeptin, 2 mM EDTA, 2 mM ethylene glycol bis(β-aminoethyl ether)-*N*,*N*,*N*′,*N*′-tetraacetic acid (EGTA), and phosphatase inhibitors (25 mM sodium fluoride, 1 mM sodium orthovanadate, 0.5 µM microcystin LR). In addition, 1 mM β-glycerophosphate was added for studying the interaction between EGFP-RepoMan and FBXW7. For in vivo ubiquitination assays, the lysis buffer was supplemented with 25 mM N-ethylmaleimide. The cell lysates were sonicated on ice water for 10 min. After centrifugation the supernatants were boiled in SDS sample buffer. For EGFP traps, cell lysates were prepared as mentioned before. To omit micrococcal nuclease treatment, we used EGFP-RepoMan-S893D (histone-binding mutant) for all the EGFP-trapping experiments (Qian *et al.*, 2015). After brief sonication (<5 min) and centrifugation, EGFP traps were performed as described previously (Van Dessel *et al.*, 2010). For the lambda phosphatase treatment, EGFP traps were treated with λ phosphatase (Santa Cruz) for 30 min at 30°C. Subsequently, the phosphatase was inhibited with 1 mM vanadate. SDS–PAGE was performed with 4–12% Bis-Tris gels (NuPAGE Invitrogen). Tris-Acetate gels (3–8%) were used for detection of His-ubiquitin. Immunoblots were visualized using ECL reagent (PerkinElmer) in an ImageQuant LAS4000 (GE Healthcare). Quantifications were performed using ImageQuant TL (GE Healthcare) using rolling-ball background subtraction. Images were cropped, and brightness and contrast were adjusted using only linear operations applied to the entire image. Final images were processed and assembled using Photoshop CS3 (Adobe). The uncropped images are provided in Supplemental Figure S8.

In vitro ubiquitination assays

Recombinant human APC/C and CDH1 were a kind gift from David Barford (MRC Laboratory of Molecular Biology, Cambridge). Poly–His-tagged RepoMan was expressed in bacteria and purified on Ni^{2+}-Sepharose. Each ubiquitination reaction contained 25 nM of recombinant APC/C, 750 nM of CDH1 and ~660 ng of purified RepoMan in a reaction medium volume of 40 µl containing 1× ubiquitin reaction buffer, 1× energy regeneration mix, 32 µM ubiquitin, 25 µM ubiquitin aldehyde, 0.25 µM recombinant UBE1, and 500 ng human UbcH10 (all reagents purchased from Boston Biochem). Ubiquitination reactions were performed for 45 min at 23°C and stopped with SDS sample buffer.

Recombinant, active SCF^{FBXW7} complex (1 µg; Millipore, 23-030) was incubated with ~660 ng of Poly–His-tagged RepoMan in a reaction volume of 40 µl (1× ubiquitin reaction buffer, 1× energy regeneration mix, 32 µM ubiquitin, 25 µM ubiquitin aldehyde, 0.25 µM recombinant UBE1, and 500 nM human UbcH3). All of these reagents were purchased from Boston Biochem. Reactions were incubated at 30°C for 90 min and terminated by the addition of SDS loading buffer and subsequently analyzed by SDS–PAGE and immunoblotting.

In vivo ubiquitination

In Supplemental Figure S4G, nonsynchronized HEK293T cells were cotransfected with EGFP-RepoMan, HA-CDH1, and His-tagged-Ubiquitin for 36 h. Cells were treated with 10 µM MG132 for 4 h before harvesting. In Supplemental Figure S5C, G1/S HEK293T cells were cotransfected with EGFP-RepoMan, 3xFlag-FBXW7α, Flag-WT-CUL1 or Flag-DN-CUL1, and His-ubiquitin. The cell lysates were prepared as described in the section *Immunoblotting and immunoprecipitation*. After preclearing with bovine serum albumin (BSA) beads, the lysate was incubated with 25 µl GFP-Trap beads for 2 h at 4°C. The beads were washed once with Tris-buffered saline, three times with 8 M urea + 1% (vol/vol) SDS in PBS (denaturing conditions) and once with 1% (vol/vol) SDS in PBS. The beads were then boiled for 5 min at 95°C in SDS sample buffer.

Immunostaining

For immunofluorescence studies, cells were consecutively grown on polylysine-coated coverslips in a 24-well chamber, fixed with 4% paraformaldehyde (PFA), permeabilized with 0.5% Triton X-100, blocked in 3% BSA/PBS, and incubated overnight at 4°C in 1.5% BSA/PBS with the primary antibodies and with secondary antibodies for 1 h at room temperature. After DNA staining with 4′,6-diamidino-2-phenylindole (DAPI), the coverslips were mounted in Mowiol onto microscope slides. Confocal images were acquired with a Leica TCS SPE laser-scanning confocal system mounted on a Leica DMI 4000B microscope and equipped with a Leica ACS APO 63× 1.30 NA oil DIC objective. All immunofluorescence images within the same experiment were acquired with identical illumination settings. Analysis of images was performed using ImageJ/Fiji (National Institutes of Health). For the quantification of mean fluorescence intensity cell borders were traced using the free hand tool in Fiji and mean pixel intensity for corresponding channel was calculated within the defined area (DAPI staining) and after subtraction of the background signal. The normalized values were plotted with Prism software, version 5.0 (GraphPad, San Diego, CA).

Time-lapse imaging and analysis

Hela Flp-In T-Rex cells were grown in a 24-well plate and transfected with siRNA against CDH1 for 48 h. Cells were arrested at the G1/S border by a single thymidine block and transgene expression was induced with 50 ng/ml Dox (Sigma-Aldrich) for at least 24 h. Cells were washed once with PBS (at least 5 h before the live assay) and grown in a modified DMEM medium containing 10% (vol/vol) FBS, 1% (vol/vol) penicillin-streptomycin, and 1% (vol/vol) Glutamax without phenol red to reduce autofluorescence. For time-lapse imaging, the Leica TCS SPE laser-scanning confocal microscope was equipped with a live-imaging chamber ensuring 37°C and 5% CO_2 and a monochrome digital camera DFC365 FX from Leica. Cells were imaged via epifluorescence and differential interference contrast (DIC) microscopy using 20× objective every 10 min. Image sequences were exported as 8-bit TIFF files for analysis in ImageJ. For quantification of mClover levels fluorescence was measured as pixel values within a region of interest (ROI) drawn around each cell using the free hand tool in Fiji and from which background pixel values were subtracted. The ROI drawn was large enough to allow for changing cell shape during mitotic exit. As fluorescence intensity varied among cells, results were presented as normalized fluorescence intensity by dividing all fluorescence intensities by the maximal fluorescence intensity and expressed as percentages. DIC images were used to determine the onset of anaphase.

Quantitative reverse transcriptase PCR

Total RNA was isolated from cells using the GenElute Mammalian Total RNA Miniprep kit from Sigma. cDNA was synthesized from 2 µg of total RNA using RevertAid Premium Reverse Transcriptase and RiboLock RNase inhibitor enzymes (Fermentas, GmBH, St. Leon-Rot, Germany) and oligo dT primers (Sigma). cDNA (1.2%) was PCR-amplified in duplicate using SYBR Green qPCR Mix (Invitrogen) and a Rotorgene detection system (Corbett Research, Cambridge, UK). Quantitative reverse transcriptase PCR was performed to check the transcript levels of *CDCA2* (5′-GCTCTCCTGAAACAAACCATCT-3′ and 5′-GCTGACTGGAAGGCTGATATT-3′). Data were normalized against the housekeeping gene GAPDH (5′-GAGTCAACGGATTTG-GTCGT-3′ and 5′-GACAAGCTTCCCGTTCTCAG-3′).

ChIP-qPCR

U2OS cells were subjected to a double-thymidine block to arrest them in G1/S. At 10 h after release from G1/S block, the cells were cross-linked with 1.5% PFA in PBS for 15 min at room temperature before stopping the reaction with 250 mM glycine for 5 min. After centrifugation (805 × *g*) for 5 min at 10°C, the pellet was resuspended in SDS lysis buffer (50 mM Tris-HCl at pH 8.0, 1% SDS, 10 mM EDTA), supplemented with 5 µM leupeptin and 0.5 mM PMSF. The resuspended pellet was sonicated during 10 min at 4°C with 30 s on/30 s off cycles. The chromatin was precleared with blocked proteinA-TSK (Affiland). ProteinA-TSK was blocked with 1 mg/ml BSA, 1 mg/ml salmon sperm DNA, and 0.5% Triton X-100. Precleared chromatin containing about 100 µg proteins was incubated overnight at 4°C with anti-FOXM1 (GTX-102170, GeneTex) or with polyclonal rabbit anti-mouse immunoglobulins (IgG). The beads were washed once with low salt buffer (16.7 mM Tris-HCl at pH 8.1, 1% Triton X-100, 167 mM NaCl, 1.2 mM EDTA, and 0.01% SDS), once with high salt buffer (20 mM Tris-HCl at pH 8.1, 1% Trition X-100, 500 mM NaCl, 0.1% SDS, and 2 mM EDTA), once with LiCl buffer (10 mM Tris-HCl at pH 8.1, 0.25 M LiCl, 1% NP-40, and 1% Na-deoxycholate), and twice with TE buffer (10 mM Tris-HCl at pH 8.0, 1 mM EDTA). The protein/DNA complex was eluted twice at 65°C with fresh elution buffer (0.1 M $NaHCO_3$ at pH 8.0, 1% SDS). After reversing the cross-links by incubation with 0.2 M NaCl and RNase A for 4 h at 65°C, the samples were treated with Proteinase K (1 h at 45°C). The purified DNA was quantified by qPCR. The primer used for ChIP-qPCR were: *ACTIN* (negative control), 5′-AGCGCGGCTACAGCTTCA-3′ and 5′-CGTAGCACAGCTTCTCCTTAATGT-3′; *AURKB* (positive control), 5′-GGGGTCCAAGGCACTGCTAC-3′ and 5′-GGGGCGGGA-GATTTGAAAAG-3′; *CDCA2*, 5′-CGGTAGGGACGGACTGATTG-3′ and 5′-GAGTCTCGCGGAGTAACGC-3′.

Cell confluency assays (IncuCyte)

Hela Flp-In T-Rex cells were plated at 7–8 × 10^3 cells per well. Confluence of the cultures was measured using IncuCyte system (Essen Biosciences, Ann Arbor, MI) over 96 h in medium containing dimethylsulfoxide (DMSO), hesperadin (S1529, Selleckchem), or AZD1152 (S1147, Selleckchem) (see Figure 7, C and D).

Bioinformatic analysis

The distribution of *CDCA2* and *AURKB* transcripts in cancers and normal tissues was analyzed using the GEPIA database (http://gepia.cancer-pku.cn/). The method used for differential analysis was one-way analysis of variance (ANOVA). The *P* value cutoff was set at <0.01. We used cBioPortal (http://www.cbioportal.org) (Gao *et al.*, 2013) to analyze the gene alteration status of *CDCA2* and *AURKB* in several types of cancer (Figure 1F). Pearson correlation coefficients were calculated for the genes of interest using function cor.test of ggpubr package in R (*P* values are based on Student's *t* distribution using function cor in R). Survival curves were calculated according to the Kaplan–Meier method (function Surv, R package survminer developed by Alboukadel Kassambara and Marcin Kosinsk; https://cran.rstudio.com/web/packages/survminer/index.html). The differences between the four cohorts of patients (Supplemental Figure S1D) were assessed using the log-rank test. The RNAseq and the clinical data of cancer patients were obtained from TCGA data sets (Colaprico *et al.*, 2016).

The function surv_cutpoint of the maxstat package in R (Hothorn and Lausen, 2002) was used to determine the optimal cut-point for the expression of *CDCA2* and *AURKB* (RNAseq) in order to categorize the groups of patients (STRATA) (Figure 1G and Supplemental Figure S1, B–D). The optimal cut-point value was calculated taking into consideration time (patients' overall survival) and event (patients' status, dead or alive) and is used to classify the gene expression: what is above the cut-off point is classified as "high" expression and what is below is classified as "low" expression.

For Figure 2D, normalized cell cycle-dependent transcript expression data from HeLa cells, synchronized with double-thymidine treatment (Santos *et al.*, 2015), were downloaded from cyclebase.org and plotted with R package ggplot2. For single-cell transcriptomic analysis (Supplemental Figure S2B), publicly available single-cell RNA-seq data sets GSE103867 (hepatocellular carcinoma) and GSE115978 (melanoma) were processed and normalized with the Seurat 2.3 package. Z-score of normalized expression data was used to calculate the Pearson correlation. For the drug sensitivity analysis (Figure 7, E and F), we analyzed cancer cell lines from CCLE with both mRNA expression and drug sensitivity (IC50) data available in GDSC (www.cancerrxgene.org/) data set. Quantile cut-off (40%) was used to stratify the high and low expression groups for both genes. The CIN level of CCLE cell lines (Supplemental Figure S7) was estimated using CIN70 signature and scored using the GSVA package from Bioconductor with the "ssGSEA" method. Data were plotted with ggboxplot function of ggpubr package in R.

Univariate and multivariate analysis

For this study, TCGA data sets from cBioPortal database (www.cbioportal.org) have been used. Cox-proportional hazards model was used to perform univariate and multivariate analysis. For each variable considered, hazard ratio, 95% CI ,and *p* value were calculated. The "high" and "low" refers to the expression of the genes *CDCA2*, *AURKB*, and *FOXM1*. These were determined through the function surv_cutpoint, as provided by the survminer R package (see additional explanation in *Bioinformatic analysis*). The statistical analyses were conducted using IBM SPSS Statistics for Mac version 25.0 (IBM, Armonk, NY), R software version 3.5.1 (R Foundation for Statistical Computing, Vienna, Austria), and GraphPad Prism ver. 7.00 for Mac (GraphPad Software, La Jolla, CA).

Mathematical modeling

We used ordinary differential equations to model the protein interactions and perform simulations and compute response curves. For the CDK1 module, we started from the model by Yang and Ferrell (Yang and Ferrell, 2013). For the Aurora-B module, we devised a set of equations based on the known feedback loops (Figure 6A). The full set of equations is

$$\frac{d[\text{Cyclin B}]}{dt} = k_s - b_{\text{deg}}\,[\text{Cyclin B}][\text{Ligase}]$$

$$\frac{d[\text{CDK1}]}{dt} = k_s + [\text{CDC25}]([\text{Cyclin B}] - [\text{CDK1}]) - [\text{WEE1}][\text{CDK1}] - b_{\text{deg}}\,[\text{CDK1}][\text{Ligase}]$$

$$\frac{d[\text{Aurora B}]}{dt} = \left(b_{CA}[\text{CDK1}] + [\text{Haspin}]\right)([\text{Total Aurora B}] - [\text{Aurora B}]) - \left(a_{RA} + b_{RA}\frac{[\text{RepoMan}]^m}{K_{RA}^m + [\text{RepoMan}]^m}\right)[\text{Aurora B}] - b_{\text{deg},A}\,[\text{Aurora B}][\text{Ligase}]$$

$$\frac{d[\text{RepoMan}]}{dt} = k_R\,([\text{Total RepoMan}] - [\text{RepoMan}]) - (b_{CR}[\text{CDK1}] + a_{AR} + b_{AR}[\text{Aurora B}])[\text{RepoMan}] - b_{\text{deg},R}[\text{RepoMan}][\text{Ligase}]$$

$$\frac{d[\text{Total Aurora B}]}{dt} = k_{s,A} - b_{\text{deg},A}\,[\text{Total Aurora B}][\text{Ligase}]$$

$$\frac{d[\text{Total RepoMan}]}{dt} = k_{s,R} - b_{\text{deg},R}[\text{Total RepoMan}][\text{Ligase}]$$

$$[\text{CDC25}] = a_{\text{CDC25}} + b_{\text{CDC25}}\frac{[\text{CDK1}]^{n_{\text{CDC25}}}}{\text{EC50}_{\text{CDC25}}^{n_{\text{CDC25}}} + [\text{CDK1}]^{n_{\text{CDC25}}}}$$

$$[\text{WEE1}] = a_{\text{WEE1}} + b_{\text{WEE1}}\frac{\text{EC50}_{\text{WEE1}}^{n_{\text{WEE1}}}}{\text{EC50}_{\text{WEE1}}^{n_{\text{WEE1}}} + [\text{CDK1}]^{n_{\text{WEE1}}}}$$

$$[\text{Haspin}] = a_{\text{Haspin}} + b_{\text{Haspin}}\frac{[\text{Aurora B}]^n}{K_{\text{Haspin}}^n + [\text{Aurora B}]^n} \qquad (1)$$

Cyclin B denotes the total amount of Cyclin B; CDK1 denotes the active form of CDK1-Cyclin B complex. The variables [Aurora B] and [RepoMan] denote the amount of active protein, whereas the variables [Total Aurora B] and [Total RepoMan] denote total abundances of these proteins. The values of CDC25, WEE1, and Haspin are taken to be simple functions of CDK1 and Aurora-B activities.

The full equation set was used only for the time series in Figure 6D. For the steady-state curve in Figure 6B, we used only the CDK1 equation, with instead of [Ligase] the function [APC/C]

$$[\text{APC/C}] = a_{\text{deg}} + b_{\text{deg}}\frac{[\text{CDK1}]^{n_{\text{deg}}}}{\text{EC50}_{\text{deg}}^{n_{\text{deg}}} + [\text{CDK1}]^{n_{\text{deg}}}} \qquad (2)$$

For the steady-state response curves for the Aurora-B module (Figure 6C), we used only the third and fourth equations above, with the total amounts constant. For the time simulations (Figure 6D), we simulated the full system, where the variable Ligase was set using timers. In Figure 6D, we used $K_{RA} = 0.125$ instead of $K_{RA} = 0.5$. We adapt this value because in our time simulation, the ratio of Aurora B to RepoMan is around 4, whereas in the isolated motif studied before, we use a base ratio of 1. This does not qualitatively change the dynamics and is just a matter of scaling. For Figure 6E, we simulated only the Aurora-B and RepoMan equations, with cosine functions for Total Aurora B, Total RepoMan, and CDK1 (see parameters in Supplemental Table S1). For Figure 6F (inhibition), we use only the Aurora-B and RepoMan equations and determined their steady state as function of I (inhibitor), where I is subtracted from the total amount of Aurora B ([Total Aurora B] – I). The vertical axis in Figure 6F is histone phosphorylation, computed as A/(1+A) where A is Aurora-B activity. Figure 6F was computed with CDK1 = 2 (high CDK1 activity), and Total Aurora B = 1. Histone levels are normalized to the value at I = 0.

Figure 8B was created using a simple model for tumor growth, with the following equations:

$$\frac{dx}{dt} = gx - dx$$

$$g(A,R) = g_l + (g_h - g_l)\frac{(A+R)^{n_g}}{K_g^{n_g} + (A+R)^{n_g}}$$

$$d(A,R) = d_h - \frac{d_h - d_l}{1 + \ln\left(\frac{A}{R}\right)^{n_d}} \qquad (3)$$

The x denotes the tumor population and g and d are growth and death rates, respectively. If $g > d$, the tumor survives. The rates depend on Aurora B and RepoMan. The functions are chosen to model two things, that both Aurora B and RepoMan separately have a positive effect on the growth rate because they suppress checkpoints. Their effects are added and a threshold is applied to obtain the growth rate. The death rate, in contrast, depends on the ratio between Aurora B and RepoMan: the death rate is small when the ratio of the proteins is one and decreases if the ratio deviates from one.

Time simulations were done using the software XPPAUT (Ermentrout, 2002). Response curves were computed using a pseudoarclength continuation algorithm written in Python and verified using the AUTO feature of XPPAUT. The model parameters are shown in Supplemental Table S1. The code to simulate the equations is available from the authors on request.

Statistical analysis

All data are representative of at least three independent repeats, unless otherwise stated. Data obtained from immunoblotting, mRNA analysis, ChIP-qPCR, or immunostaining analysis are expressed as means ± SD. Data obtained from ChIP qPCRs were normally distributed. No statistical methods were used to predetermine sample size. Two-tailed Student's *t* tests were conducted using the Prism software, version 5.0 (GraphPad, San Diego, CA), and *P* values <0.05 were considered significant. Correlations were analyzed by Pearson's correlation coefficient (*r*). One-way ANOVA, log-rank test,

and Wilcoxon–Mann–Whitney Test were utilized as appropriate (see *Bioinformatic analysis*).

Data availability

The authors declare that all the data supporting the findings of this study are available within the article and from the corresponding author upon reasonable request.

ACKNOWLEDGMENTS

This work was supported by the Fund for Scientific Research-Flanders (Grants G.0B9917N and G0A5217N, as well as individual support for Jan Rombouts), a Flemish Concerted Research Action (GOA/15/016), and the Belgian Foundation Against Cancer. Annemie Hoogmartens and Gerd Van der Hoeven provided technical assistance. We thank David Barford (MRC Laboratory of Molecular Biology, Cambridge, UK) for providing purified APC and CDH1 and Aleyde van Eynde (KU Leuven, Belgium) for expert advice on FOXM1 ChIP assays. We thank the HPA project team for making the valuable collection of IHC images publicly available.

REFERENCES

Akhoondi S, Sun D, Von Der Lehr N, Apostolidou S, Klotz K, Maljukova A, Cepeda D, Fiegl H, Dofou D, Marth C, *et al.* (2007). FBXW7/hCDC4 is a general tumor suppressor in human cancer. Cancer Res 67, 9006–9012.

Barretina J, Caponigro G, Stransky N, Venkatesan K, Margolin AA, Kim S, Wilson CJ, Lehár J, Kryukov GV, Sonkin D, *et al.* (2012). The Cancer Cell Line Encyclopedia enables predictive modelling of anticancer drug sensitivity. Nature 483, 603–607.

Blom N, Sicheritz-Pontén T, Gupta R, Gammeltoft S, Brunak S (2004). Prediction of post-translational glycosylation and phosphorylation of proteins from the amino acid sequence. Proteomics 4, 1633–1649.

Bonet C, Giuliano S, Ohanna M, Bille K, Allegra M, Lacour JP, Bahadoran P, Rocchi S, Ballotti R, Bertolotto C (2012). Aurora B is regulated by the mitogen-activated protein kinase/extracellular signal-regulated kinase (MAPK/ERK) signaling pathway and is a valuable potential target in melanoma cells. J Biol Chem 287, 29887–29898.

Borisa AC, Bhatt HG (2017). A comprehensive review on Aurora kinase: Small molecule inhibitors and clinical trial studies. Eur J Med Chem 140, 1–19.

Brandeis M and Hunt T (1996). The proteolysis of mitotic cyclins in mammalian cells persists from the end of mitosis until the onset of S phase. EMBO J 15, 5280–5289.

Britigan EMC, Wan J, Zasadil LM, Ryan SD, Weaver BA (2014). The ARF tumor suppressor prevents chromosomal instability and ensures mitotic checkpoint fidelity through regulation of Aurora B. Mol Biol Cell 25, 2761–2773.

Cappell SD, Chung M, Jaimovich A, Spencer SL, Meyer T (2016). Irreversible APCCdh1 inactivation underlies the point of no return for cell-cycle entry. Cell 166, 167–180.

Carmena M, Wheelock M, Funabiki H, Earnshaw WC (2012). The chromosomal passenger complex (CPC): From easy rider to the godfather of mitosis. Nat Rev Mol Cell Biol 13, 789–803.

Carter SL, Eklund AC, Kohane IS, Harris LN, Szallasi Z (2006). A signature of chromosomal instability inferred from gene expression profiles predicts clinical outcome in multiple human cancers. Nat Genet 38, 1043–1048.

Cimini D, Wan X, Hirel CB, Salmon ED (2006). Aurora kinase promotes turnover of kinetochore microtubules to reduce chromosome segregation errors. Curr Biol 16, 1711–1718.

Colaprico A, Silva TC, Olsen C, Garofano L, Cava C, Garolini D, Sabedot TS, Malta TM, Pagnotta SM, Castiglioni I, *et al.* (2016). TCGAbiolinks: An R/Bioconductor package for integrative analysis of TCGA data. Nucleic Acids Res 44, e71.

Crusio KM, King B, Reavie LB, Aifantis I (2010). The ubiquitous nature of cancer: The role of the SCFFbw7 complex in development and transformation. Oncogene 29, 4865–4873.

Davis DB, Lavine JA, Suhonen JI, Krautkramer KA, Rabaglia ME, Sperger JM, Fernandez LA, Yandell BS, Keller MP, Wang IM, *et al.* (2010). FoxM1 is up-regulated by obesity and stimulates β-cell proliferation. Mol Endocrinol 24, 1822–1834.

Davis RJ, Welcker M, Clurman BE (2014). Tumor suppression by the Fbw7Ubiquitin ligase: Mechanisms and opportunities. Cancer Cell 26, 455–464.

De Castro IJ, Budzak J, Di Giacinto ML, Ligammari L, Gokhan E, Spanos C, Moralli D, Richardson C, De Las Heras JI, Salatino S, *et al.* (2017). Repo-Man/PP1 regulates heterochromatin formation in interphase. Nat Commun 8, 14048.

Dephoure N, Zhou C, Villén J, Beausoleil SA, Bakalarski CE, Elledge SJ, Gygi SP (2008). A quantitative atlas of mitotic phosphorylation. Proc Natl Acad Sci USA 105, 10762–10767.

Ermentrout GB (2002). Simulating, analysing, and animating dymaical systems: a guide to XPPAUT for researchers and students. Books .google.com 14. https://doi.org/10.1137/1.9780898718195.

Ferrell JE (2013). Feedback loops and reciprocal regulation: Recurring motifs in the systems biology of the cell cycle. Curr Opin Cell Biol 25, 676–686.

Fischer M, Quaas M, Steiner L, Engeland K (2016a). The p53-p21-DREAM-CDE/CHR pathway regulates G2/M cell cycle genes. Nucleic Acids Res 44, 164–174.

Fischer M, Grossmann P, Padi M, DeCaprio JA (2016b). Integration of TP53, DREAM, MMB-FOXM1 and RB-E2F target gene analyses identifies cell cycle gene regulatory networks. Nucleic Acids Res 44, 6070–6086.

Gao J, Aksoy BA, Dogrusoz U, Dresdner G, Gross B, Sumer SO, Sun Y, Jacobsen A, Sinha R, Larsson E, *et al.* (2013). Integrative analysis of complex cancer genomics and clinical profiles using the cBioPortal. Sci Signal 6, pl1.

Gelens L, Qian J, Bollen M, Saurin AT (2018). The importance of kinase–phosphatase integration: lessons from mitosis. Trends Cell Biol 28, 6–21.

González-Loyola A, Fernández-Miranda G, Trakala M, Partida D, Samejima K, Ogawa H, Cañamero M, de Martino A, Martínez-Ramírez Á, de Cárcer G, *et al.* (2015). Aurora B overexpression causes aneuploidy and p21 Cip1 repression during tumor development. Mol Cell Biol 35, 3566–3578.

Gully CP, Velazquez-Torres G, Shin JH, Fuentes-Mattei E, Wang E, Carlock C, Chen J, Rothenberg D, Adams HP, Choi HH, *et al.* (2012). Aurora B kinase phosphorylates and instigates degradation of p53. Proc Natl Acad Sci USA 109, E1513–E1522.

Hauf S, Cole RW, LaTerra S, Zimmer C, Schnapp G, Walter R, Heckel A, Van Meel J, Rieder CL, Peters JM (2003). The small molecule Hesperadin reveals a role for Aurora B in correcting kinetochore-microtubule attachment and in maintaining the spindle assembly checkpoint. J Cell Biol 161, 281–294.

He J, Chao WCH, Zhang Z, Yang J, Cronin N, Barford D (2013). Insights into degron recognition by APC/C coactivators from the structure of an Acm1-Cdh1 complex. Mol Cell 50, 649–660.

Hindriksen S, Lens SMA, Hadders MA (2017). The ins and outs of Aurora B inner centromere localization. Front Cell Dev Biol 5, 112.

Hoffmann I, Clarke PR, Marcote MJ, Karsenti E, Draetta G (1993). Phosphorylation and activation of human cdc25-C by cdc2–cyclin B and its involvement in the self-amplification of MPF at mitosis. EMBO J 12, 53–63.

Hothorn T, Lausen B (2002). Maximally selected rank statistics in {R}. R News. https://cran.r-project.org/web/packages/maxstat/vignettes/maxstat.pdf.

Jerby-Arnon L, Shah P, Cuoco MS, Rodman C, Su MJ, Melms JC, Leeson R, Kanodia A, Mei S, Lin JR, *et al.* (2018). A cancer cell program promotes T cell exclusion and resistance to checkpoint blockade. Cell 175, 984–997.e24.

Kelly AE, Ghenoiu C, Xue JZ, Zierhut C, Kimura H, Funabiki H (2010). Survivin reads phosphorylated histone H3 threonine 3 to activate the mitotic kinase Aurora B. Science 330, 235–239.

Kelly AE, Sampath SC, Maniar TA, Woo EM, Chait BT, Funabiki H (2007). Chromosomal enrichment and activation of the aurora b pathway are coupled to spatially regulate spindle assembly. Dev Cell 12, 31–43.

Kimura M, Uchida C, Takano Y, Kitagawa M, Okano Y (2004). Cell cycle-dependent regulation of the human aurora B promoter. Biochem Biophys Res Commun 316, 930–936.

Kireeva N, Lakonishok M, Kireev I, Hirano T, Belmont AS (2004). Visualization of early chromosome condensation: a hierarchical folding, axial glue model of chromosome structure. J Cell Biol 166, 775–785.

Koepp DM, Schaefer LK, Ye X, Keyomarsi K, Chu C, Harper JW, Elledge SJ (2001). Phosphorylation-dependent ubiquitination of cyclin E by the SCF FBW7 ubiquitin ligase. Science 294, 173–177.

Krasnoselsky AL, Whiteford CC, Wei JS, Bilke S, Westermann F, Chen QR, Khan J (2005). Altered expression of cell cycle genes distinguishes aggressive neuroblastoma. Oncogene 24, 1533–1541.

Kumar GS, Gokhan E, De Munter S, Bollen M, Vagnarelli P, Peti W, Page R (2016). The Ki-67 and RepoMan mitotic phosphatases assemble via an identical, yet novel mechanism. Elife 5, e16539.

Lagarde P, Przybyl J, Brulard C, Pérot G, Pierron G, Delattre O, Sciot R, Wozniak A, Schöffski P, Terrier P, *et al.* (2013). Chromosome instability

accounts for reverse metastatic outcomes of pediatric and adult synovial sarcomas. J Clin Oncol 31, 608–615.
Lehman NL, Verschuren EW, Hsu JY, Cherry AM, Jackson PK (2006). Overexpression of the anaphase promoting complex/cyclosome inhibitor Emi1 leads to tetraploidy and genomic instability of p53-deficient cells. Cell Cycle 5, 1569–1573.
Löwenberg B, Muus P, Ossenkoppele G, Rousselot P, Cahn JY, Ifrah N, Martinelli G, Amadori S, Berman E, Sonneveld P, *et al*. (2011). Phase 1/2 study to assess the safety, efficacy, and pharmacokinetics of barasertib (AZD1152) in patients with advanced acute myeloid leukemia. Blood 118, 6030–6036.
Lv D, Li Y, Zhang W, Alvarez AA, Song L, Tang J, Gao WQ, Hu B, Cheng SY, Feng H (2017). TRIM24 is an oncogenic transcriptional co-activator of STAT3 in glioblastoma. Nat Commun 8, 1454.
Mross K, Richly H, Frost A, Scharr D, Nokay B, Graeser R, Lee C, Hilbert J, Goeldner RG, Fietz O, *et al*. (2016). A phase I study of BI 811283, an Aurora B kinase inhibitor, in patients with advanced solid tumors. Cancer Chemother Pharmacol 78, 405–417.
Müller GA, Wintsche A, Stangner K, Prohaska SJ, Stadler PF, Engeland K (2014). The CHR site: Definition and genome-wide identification of a cell cycle transcriptional element. Nucleic Acids Res 42, 10331A–10350A.
Nakayama KI, Nakayama K (2006). Ubiquitin ligases: Cell-cycle control and cancer. Nat Rev Cancer 6, 369–381.
Nguyen HG, Chinnappan D, Urano T, Ravid K (2005). Mechanism of Aurora-B degradation and its dependency on intact KEN and A-boxes: identification of an aneuploidy-promoting property. Mol Cell Biol 25, 4977–4992.
Nijenhuis W, Vallardi G, Teixeira A, Kops GJPL, Saurin AT (2014). Negative feedback at kinetochores underlies a responsive spindle checkpoint signal. Nat Cell Biol 16, 1257–1264.
Olsen JV, Vermeulen M, Santamaria A, Kumar C, Miller ML, Jensen LJ, Gnad F, Cox J, Jensen TS, Nigg EA, *et al*. (2010). Quantitative phosphoproteomics revealswidespread full phosphorylation site occupancy during mitosis. Sci Signal 3, ra3.
Ota T, Suto S, Katayama H, Han ZB, Suzuki F, Maeda M, Tanino M, Terada Y, Tatsuka M (2002). Increased mitotic phosphorylation of histone H3 attributable to AIM-1/aurora-B overexpression contributes to chromosome number instability. Cancer Res 62, 5168–5177.
Parker LL, Piwnica-Worms H (1992). Inactivation of the p34cdc2-Cyclin B complex by the human WEE1 tyrosine kinase. Science 257, 1955–1957.
Peng A, Lewellyn AL, Schiemann WP, Maller JL (2010). Repo-Man controls a protein phosphatase 1-dependent threshold for DNA damage checkpoint activation. Curr Biol 20, 387–396.
Peters JM (2006). The anaphase promoting complex/cyclosome: a machine designed to destroy. Nat Rev Mol Cell Biol 7, 644–656.
Phan NN, Wang C, Li K, Chen C (2018). Distinct expression of CDCA3, CDCA5, and CDCA8 leads to shorter relapse free survival in breast cancer patient. Oncotarget 9, 6977–6992.
Pines J (2011). Cubism and the cell cycle: The many faces of the APC/C. Nat Rev Mol Cell Biol 12, 427–438.
Pomerening JR, Sontag ED, Ferrell JE (2003). Building a cell cycle oscillator: Hysteresis and bistability in the activation of Cdc2. Nat Cell Biol 5, 346–351.
Prévost M, Chamousset D, Nasa I, Freele E, Morrice N, Moorhead G, Trinkle-Mulcahy L (2013). Quantitative "Fragmentome" mapping reveals novel, domain-specific partners for the modular protein RepoMan (Recruits PP1 onto mitotic chromatin at anaphase). Mol Cell Proteomics 12, 1468–1486.
Qian J, Lesage B, Beullens M, Van Eynde A, Bollen M (2011). PP1/repo-man dephosphorylates mitotic histone H3 at T3 and regulates chromosomal aurora B targeting. Curr Biol 21, 766–773.
Qian J, Beullens M, Huang J, De Munter S, Lesage B, Bollen M (2015). Cdk1 orders mitotic events through coordination of a chromosome-associated phosphatase switch. Nat Commun 6, 10215.
Qian J, Beullens M, Lesage B, Bollen M (2013). Aurora B defines its own chromosomal targeting by opposing the recruitment of the phosphatase scaffold Repo-Man. Curr Biol 23, 1136–1143.
Rambout X, Detiffe C, Bruyr J, Mariavelle E, Cherkaoui M, Brohée S, Demoitié P, Lebrun M, Soin R, Lesage B, *et al*. (2016). The transcription factor ERG recruits CCR4-NOT to control mRNA decay and mitotic progression. Nat Struct Mol Biol 23, 663–672.
Raychaudhuri P, Park HJ (2011). FoxM1: a master regulator of tumor metastasis. Cancer Res 71, 4329–4333.
Ryu B, Kim DS, DeLuca AM, Alani RM (2007). Comprehensive expression profiling of tumor cell lines identifies molecular signatures of melanoma progression. PLoS One 2, e594.
Sansregret L, Vanhaesebroeck B, Swanton C (2018). Determinants and clinical implications of chromosomal instability in cancer. Nat Rev Clin Oncol 15, 139–150.
Santos A, Wernersson R, Jensen LJ (2015). Cyclebase 3.0: A multi-organism database on cell-cycle regulation and phenotypes. Nucleic Acids Res 43, D1140–D1144.
Schwartz GK, Carvajal RD, Midgley R, Rodig SJ, Stockman PK, Ataman O, Wilson D, Das S, Shapiro GI (2013). Phase i study of barasertib (AZD1152), a selective inhibitor of Aurora B kinase, in patients with advanced solid tumors. Invest New Drugs 31, 370–380.
Sessa F, Mapelli M, Ciferri C, Tarricone C, Areces LB, Schneider TR, Stukenberg PT, Musacchio A (2005). Mechanism of Aurora B activation by INCENP and inhibition by hesperadin. Mol Cell 18, 379–391.
Sha W, Moore J, Chen K, Lassaletta AD, Yi C-S, Tyson JJ, Sible JC (2003). Hysteresis drives cell-cycle transitions in Xenopus laevis egg extracts. Proc Natl Acad Sci USA 100, 975–980.
Shi R, Zhang C, Wu Y, Wang X, Sun Q, Sun J (2017). CDCA2 promotes lung adenocarcinoma cell proliferation and predicts poor survival in lung adenocarcinoma patients. Oncotarget 8, 19768–19779.
Sivakumar S, Gorbsky GJ (2015). Spatiotemporal regulation of the anaphase-promoting complex in mitosis. Nat Rev Mol Cell Biol 16, 82–94.
Stewart S, Fang G (2005). Destruction box-dependent degradation of Aurora B is mediated by the anaphase-promoting complex/cyclosome and Cdh1. Cancer Res 65, 8730–8735.
Tang A, Gao K, Chu L, Zhang R, Yang J, Zheng J (2017). Aurora kinases: Novel therapy targets in cancers. Oncotarget 8, 23937–23954.
Teng CL, Hsieh YC, Phan L, Shin J, Gully C, Velazquez-Torres G, Skerl S, Yeung SCJ, Hsu SL, Lee MH (2012). FBXW7 is involved in Aurora B degradation. Cell Cycle 11, 4059–4068.
Thornton BR, Toczyski DP (2006). Precise destruction: An emerging picture of the APC. Genes Dev. 20, 3069–3078.
Trinkle-Mulcahy L, Andersen J, Yun WL, Moorhead G, Mann M, Lamond AI (2006). Repo-Man recruits PP1γ to chromatin and is essential for cell viability. J Cell Biol 172, 679–692.
Tsukahara T, Tanno Y, Watanabe Y (2010). Phosphorylation of the CPC by Cdk1 promotes chromosome bi-orientation. Nature 467, 719–23.
Uchida F, Uzawa K, Kasamatsu A, Takatori H, Sakamoto Y, Ogawara K, Shiiba M, Bukawa H, Tanzawa H (2013). Overexpression of CDCA2 in human squamous cell carcinoma: correlation with prevention of G1 phase arrest and apoptosis. PLoS One 8, 1–9.
Vagnarelli P, Hudson DF, Ribeiro SA, Trinkle-Mulcahy L, Spence JM, Lai F, Farr CJ, Lamond AI, Earnshaw WC (2006). Condensin and Repo-Man-PP1 co-operate in the regulation of chromosome architecture during mitosis. Nat Cell Biol 8, 1133–1142.
Vagnarelli P, Ribeiro S, Sennels L, Sanchez-Pulido L, de Lima Alves F, Verheyen T, Kelly DA, Ponting CP, Rappsilber J, Earnshaw WC (2011). Repo-Man coordinates chromosomal reorganization with nuclear envelope reassembly during mitotic exit. Dev Cell 21, 328–342.
Van Dessel N, Beke L, Görnemann J, Minnebo N, Beullens M, Tanuma N, Shima H, Van Eynde A, Bollen M (2010). The phosphatase interactor NIPP1 regulates the occupancy of the histone methyltransferase EZH2 at Polycomb targets. Nucleic Acids Res 38, 7500–7512.
Vergassola M, Deneke VE, Talia SDi (2018). Mitotic waves in the early embryogenesis of Drosophila: Bistability traded for speed. Proc Natl Acad Sci USA 115, E2165–E2174.
Wan L, Chen M, Cao J, Dai X, Yin Q, Zhang J, Song SJ, Lu Y, Liu J, Inuzuka H, *et al*. (2017). The APC/C E3 ligase complex activator fzr1 restricts braf oncogenic function. Cancer Discov 7, 424–441.
Wang I-C, Chen Y-J, Hughes D, Petrovic V, Major ML, Park HJ, Tan Y, Ackerson T, Costa RH (2005). Forkhead box M1 regulates the transcriptional network of genes essential for mitotic progression and genes encoding the SCF (Skp2-Cks1) ubiquitin ligase. Mol Cell Biol 25, 10875–10894.
Wang F, Ulyanova NP, Van Der Waal MS, Patnaik D, Lens SMA, Higgins JMG (2011). A positive feedback loop involving haspin and aurora B promotes CPC accumulation at centromeres in mitosis. Curr Biol 21, 1061–1069.
Wang Y, Ung MH, Xia T, Cheng W, Cheng C (2017). Cancer cell line specific co-factors modulate the FOXM1 cistrome. Oncotarget 8, 76498–76515.
Welcker M, Orian A, Grim JA, Eisenman RN, Clurman BE (2004). A nucleolar isoform of the Fbw7 ubiquitin ligase regulates c-Myc and cell size. Curr Biol 14, 1852–1857.

Whitfield ML, Sherlock G, Saldanha AJ, Murray JI, Ball CA, Alexander KE, Matese JC, Perou CM, Hurt MM, Brown PO, *et al*. (2002). Identification of genes periodically expressed in the human cell cycle and their expression in tumors. Mol Biol Cell 13, 1977–2000.

Wu L, Ma CA, Zhao Y, Jain A (2011). Aurora B interacts with NIR-p53, leading to p53 phosphorylation in its DNA-binding domain and subsequent functional suppression. J Biol Chem 286, 2236–2244.

Wu D, De Wever V, Derua R, Winkler C, Beullens M, Van Eynde A, Bollen M (2018). A substrate-trapping strategy for protein phosphatase PP1 holoenzymes using hypoactive subunit fusions. J Biol Chem 293, 15152–15162.

Wurzenberger C, Held M, Lampson MA, Poser I, Hyman AA, Gerlich DW (2012). Sds22 and repo-man stabilize chromosome segregation by counteracting Aurora B on anaphase kinetochores. J Cell Biol 198, 173–183.

Yang Q, Ferrell JE (2013). The Cdk1-APC/C cell cycle oscillator circuit functions as a time-delayed, ultrasensitive switch. Nat Cell Biol 15, 519–525.

Yang W, Soares J, Greninger P, Edelman EJ, Lightfoot H, Forbes S, Bindal N, Beare D, Smith JA, Thompson IR, *et al.* (2013). Genomics of Drug Sensitivity in Cancer (GDSC): a resource for therapeutic biomarker discovery in cancer cells. Nucleic Acids Res 41, D955–D961.

Zaytsev AV, Segura-Pena D, Godzi M, Calderon A, Ballister ER, Stamatov R, Mayo AM, Peterson L, Black BE, Ataullakhanov FI, *et al.* (2016). Bistability of a coupled Aurora B kinase-phosphatase system in cell division. Elife 5, e10644.

Zheng H, Pomyen Y, Hernandez MO, Li C, Livak F, Tang W, Dang H, Greten TF, Davis JL, Zhao Y, *et al*. (2018). Single-cell analysis reveals cancer stem cell heterogeneity in hepatocellular carcinoma. Hepatology 68, 127–140.

Zhou L, Chen J, Li Z, Li X, Hu X, Huang Y, Zhao X, Liang C, Wang Y, Sun L, *et al.* (2010). Integrated profiling of MicroRNAs and mRNAs: MicroRNAs Located on Xq27.3 associate with clear cell renal cell carcinoma. PLoS One 5, e15224.

Zhou L, Tian X, Zhu C, Wang F, Higgins JM (2014). Polo-like kinase-1 triggers Histone phosphorylation by Haspin in mitosis. EMBO Rep. 15, 273–281.